Why does the magnetotail reconnection have significantly varying strength of fluctuation?

Runqing Jin[1,2], Meng Zhou[2,3,4*], Bin Yin[2,3], Yongyuan Yi[2,3], Zhihong Zhong[2,3,4], Ye Pang[2], Xiaohua Deng[2,4]

[1] School of Resources and Environment, Nanchang University, Nanchang, China

[2] Institute of Space Science and Technology, Nanchang University, Nanchang, China

[3] School of Physics and Materials Science, Nanchang University, Nanchang, China

[4] Engineering Research Center of Intelligent Sensing Technology in Space Information, Ministry of Education, Nanchang, China

*Corresponding author: monmentum82@gmail.com

Abstract

Magnetic reconnection in the Earth's magnetosphere is usually manifested as a turbulent state in which the large amplitude fluctuations disrupt the main reconnection layer, while it occasionally shows a clear structured reconnection layer with weak fluctuations, i.e., a laminar state. To understand why the fluctuation strength varies significantly among reconnection in the Earth's magnetotail, we have examined tens of reconnection events in the Earth's magnetotail observed by the Magnetospheric Multi-Scale (MMS) mission. We primarily examine the correlation between fluctuation strength in reconnection, quantified by dB_{rec} and dE_{rec}, and reconnection inflow conditions and upstream solar wind conditions. The fluctuation strength (dB_{rec}, dE_{rec}) for these reconnections ranges from 0.7 to 10 nT and 0.8 to 30 mV/m, respectively. Our analysis unveils significant correlations between inflow conditions including Alfven speed $V_{A,in}$, β_{in}, magnetic disturbances dB_{in} and electric field disturbances dE_{in} with (dB_{rec}, dE_{rec}). Fluctuation strength also shows good correlations with interplanetary magnetic field (IMF) cone angle and solar wind dynamic pressure, whereas it has an unclear relationship with substorm and storm activities. We suggest that inflow reconnection conditions act as the principal catalysts for turbulence during reconnection.

Plain Language Summary

Turbulence and reconnection are closely intertwined phenomena. When turbulence is present during reconnection, it often manifests as a distinct turbulent state. Strong turbulent reconnection plays a vital role in energy conversion and particle acceleration. However, the factors causing significant variations in the fluctuation strength of reconnection remain unclear. In this study, we conducted a statistical analysis of the fluctuation strength of 31 reconnection events in the magnetotail. Our findings indicate that the inflow parameters of reconnection are pivotal in determining fluctuation strength. Additionally, solar wind dynamic pressure and IMF cone angle also influence the disturbance amplitude of reconnection. These insights contribute to a deeper understanding of the mechanisms that drive the evolution of reconnection into turbulence.

Key Points:

- Parameters in the reconnection inflow region play a pivotal role in determining the fluctuation strength in reconnection.
- Reconnection tends to be more turbulent when the IMF is southward and solar wind pressure is large.
- The strength of fluctuation in reconnection does not directly impact the intensity of substorm and magnetic storm.

1. Introduction

Magnetic reconnection is a fundamental plasma phenomenon occurring across diverse plasma settings, including astrophysical, solar, geophysical, and laboratory plasmas. This process rapidly converts magnetic energy into kinetic and thermal energy by altering the magnetic field topology (Parker, 1957; Sonnerup, 1984; Schindler et al., 1988; Zhou et al., 2019a). Within turbulent plasma, such as the magnetosheath downstream of the bow shock, notable oscillations in both the plasma density and magnetic field are frequently observed. These oscillations induce thin current sheets,

which in turn serve as a precursor to reconnection processes, leading to turbulent energization of plasma through energy dissipation (Retinò et al., 2007; Sundkvist et al., 2007).

Reconnection can also drive turbulence and spontaneously evolve into a turbulent state. 3-D simulations of reconnection show a heightened level of complexity and turbulence compared to 2-D simulation because the additional degree of freedom in the third direction facilitates the growth of many instabilities and wave modes. Che et al. (2010) find that the turbulent evolution of reconnection creates a web of filamentary currents, disrupting the main reconnecting current sheet. Daughton et al. (2011) demonstrate that the generation of numerous small-scale magnetic flux ropes, driven by secondary tearing instabilities, induces strong turbulence within the entire reconnection layer (Daughton et al., 2011). In addition, lower-hybrid drift instability (Yin et al., 2008; Divin et al., 2015; Price et al., 2016; 2017; Zhou et al., 2009a, 2009b; 2018) and interchange instability (Lapenta & Bettarini, 2011; Lapenta et al., 2015, 2018, 2020; Pucci et al., 2017) caused by strong density gradient in the outflow region can produce turbulence in reconnection. Kelvin-Helmholtz instability, driven by either ion or electron flow shear, can be a potential source for turbulence in reconnection (Zhong et al., 2018). Kinetic instabilities driven by non-Maxwellian particle velocity distribution functions also contribute to the development of turbulence in reconnection (Ergun et al., 2018; Khotyaintsev et al., 2020; Yoon et al., 2005; Zhong et al., 2021).

Turbulent reconnection has been extensively documented through in-situ spacecraft observations in various regions, including the Earth's magnetosphere and solar wind (Eastwood et al., 2009; Chaston et al., 2009; Huang et al., 2010, 2012; Osman et al., 2015; Zhou et al., 2021; Ergun et al., 2020; Li et al., 2022; Vörös et al., 2014; Osman et al., 2014; Wang et al., 2022). In these observations, turbulent reconnection is generally identified or characterized by significant disturbances in the electromagnetic fields and power-law magnetic field spectrum.

More recently, the role of turbulence in magnetic reconnection has been intensively investigated. It has been illustrated that turbulent reconnection efficiently drives the conversion of magnetic energy into plasma kinetic energy in an intermittent manner

(Sun et al., 2022; Lu et al., 2023; Jin et al., 2022, 2024; Osman et al., 2015). The substantial energy dissipation during turbulent reconnection predominantly occurs within kinetic-scale coherent structures (Fu et al., 2017; Bergstedt et al., 2020; Zhou et al., 2021; Huang et al., 2021; Jin et al., 2024). Fu et al. (2017) discovered that energy dissipation in magnetic reconnection primarily occurs at the O-point rather than the X-point, and turbulence can enhance the energy conversion within current sheets. Zhou et al. (2021) find that electron-scale current sheets are formed in turbulent reconnection outflow region. Some of the current sheets are reconnecting, which contributes substantially to the overall energy release during the large-scale reconnection. Ergun et al. (2020) suggest that the presence of magnetic holes in strong turbulence can effectively trap particles and lead to significant non-thermal particle acceleration. Lazarian and Vishniac (1999) propose that turbulent reconnection with stochastic magnetic field lines can substantially increase the reconnection rate.

On the other hand, waves may be important in the energy budget of turbulent reconnection. It has been shown that the dominant wave mode in turbulent reconnection is the fast mode or Alfvén-whistler mode (Eastwood et al., 2009; Huang et al., 2010; 2012). This underscores the pivotal role of waves in the energy cascade and dissipation in turbulence driven by magnetic reconnection. Whether plasma waves or coherent structures play the dominant role in energy dissipation in turbulent reconnection is unclear.

Another interesting question arises from the observational view of point: why do certain reconnection events manifest as weak fluctuations, indicative of laminar states, while others show substantial amplitude perturbations? For instance, the reconnection events studied by Torbert et al. (2018) and Zhou et al. (2019a, b) exhibit relatively small amplitude fluctuation in the magnetic field, characterized by well-structured reconnection layers (Torbert et al., 2018; Zhou et al., 2019a, 2019b). Conversely, in some other reconnection events (Ergun et al., 2018, 2020, 2022; Zhou et al., 2021), both the magnetic and electric fields exhibit prominent disturbances and rapid fluctuations, disrupting the structured reconnection layers. In such instances, remarkably large electric fields, currents, and significant increases in energetic electrons are frequently

observed. Motivated by these observations, this study aims to delve deeper into the factors determining the fluctuation strength of reconnection. In other words, we attempt to understand the mechanisms underlying the generation of turbulence during reconnection. Therefore, we statistically analyze 31 reconnection events in the Earth's magnetotail, exploring the relationship between fluctuation strengths and factors such as reconnection inflow conditions, upstream solar wind conditions, and geomagnetic activities.

2. Instrumentation

For this study, we employed a combination of measurements from the MMS satellite, utilizing instruments such as the Flux Gate Magnetometer (FGM) for magnetic field measurements (Russell et al., 2016; Ergun et al., 2016), the Electric Double Probes (EDP) for electric field measurements (Lindqvist et al., 2016; Torbert et al., 2016), and the Fast Plasma Investigation (FPI) for plasma moments (Pollock et al., 2016). This work specifically utilized Fast mode data since the high-resolution burst mode data from the MMS was unnecessary for assessing fluctuation strengths and inflow conditions in these events.

In the magnetotail, the plasma density is relatively low, particularly in the reconnection outflow region where the plasma is exhausted. In such an environment, the corrected phase space density tends to have negative values after eliminating photoelectrons from the low phase space density measured by FPI (Gershman et al., 2017). This results in abnormally large outliers in electron density (n_e) and temperature (T_e). Considering this issue, we utilize partial ion and electron moment data provided directly by FPI. For electrons, we used partial moment data for energies surpassing 50 eV, which is greater than the energy of photoelectrons generated within the Dual Electron Spectrometers (DES) by solar extreme ultraviolet (EUV) photons (Gershman et al., 2017). The presence of these photoelectrons, independent of spacecraft potential, introduces difficulties in measuring low-energy electrons (< 50 eV). For ions, partial moment data for energies exceeding 250 eV were used, as penetrating radiation below

250 eV maintains a nearly constant background flux (Gershman et al., 2019). Crucially, the partial moment data yields a near equality in electron and ion densities. The solar wind and Interplanetary Magnetic Field (IMF) parameters are derived from the OMNI database with a time resolution of 1 min (http://sdaweb.gsfc.nasa.gov/cdaweb/istp_public/). The OMNI solar wind data has been time-shifted to the Earth's bow shock nose. The auroral electrojet lower (AL) index is measured through ground stations within The Time History of Events and Macroscale Interactions during Substorms (THEMIS) mission network (Angelopoulos, 2008).

3. Observations of turbulent reconnection: a case study

We present two magnetotail reconnection events observed by MMS, each illustrating a different strength of turbulence, to elucidate the methods employed in our statistical analysis. Specifically, we categorize magnetotail reconnection into two types: plasma sheet reconnection (PSR) and lobe reconnection (LR). Here, we stipulate that the LR must meet the following conditions: (1) The electron temperature (T_e) demonstrates a pronounced enhancement relative to the neighboring region, with the peak T_e exceeding four times that of the surrounding region; (2) The electron density (n_e) drops to a very low value compared to the adjacent region; (3) A corresponding increase in the Alfvén speed (V_{Ax}). Conditions not meeting the aforementioned criteria are classified as PSR.

3.1 Magnetotail plasma sheet Reconnection: 2017-06-19 event

Figure 1(a1) – (a9) provides an overview of PSR observed by MMS1 from 09:30 to 10:00 UT on June 19, 2017 (reported by Zhou et al., 2019b). During this interval, a bulk flow reversal is evident, transitioning from negative to positive (Figure 1(a4)) and the reversal of the magnetic field B_z from negative to positive (Figure 1(a1), suggesting MMS traversed a tailward-retreating X-line. An ion diffusion region (IDR) is observed around 09:43:25 UT (Zhou et al., 2019b). The fluctuation level of the magnetic field is relatively weak. Moreover, there is no significant density decrease and T_e remains stable in the outflow region. V_{Ax} is between 500 and 1000 km/s, with a maximum electric

field of approximately 40 mV/m, collectively indicating this is a PSR.

A reconnection inflow region was encountered by MMS at ~ 09:41 UT. The inflow region is manifested as noticeable density decreases, large $|B_x|$ (> 10 nT), absence of ion outflow, and a sudden decrease in electron flux. Although similar features to the inflow region were observed around 09:45 UT, a strong electric field indicates that the satellite was crossing the separatrix region. Hence, we consider the period around 09:41 UT as the inflow region, marked by a black vertical line in Figure 1(a). Our analysis focuses on the highlighted blue region, from the onset of outflow at ~ 09:35 UT to its disappearance at ~ 09:51 UT, to compute the fluctuation strength associated with reconnection. To mitigate any interference from the inflow region that might influence the fluctuation strength associated with reconnection, we intentionally exclude the previously defined inflow region.

3.2 The Transition from Magnetotail Plasma Sheet Reconnection to Lobe Reconnection: 2019-09-06 event

Figure 1(b1) – (b9) provides an observation of the transition from the magnetotail PSR to LR observed from 04:20 to 04:50 UT on September 6, 2019. Before 04:35 UT, the magnetic field disturbance was subdued, and T_e remained stable at around 1 keV. After 04:35 UT, drastic magnetic field variations were observed (see Figure 1(b1)). During this period, T_e rapidly increased from 1 keV to 10 keV (Figure 1(b6)), accompanied by a notable decrease in density from 0.3 cm^{-3} to less than 0.1 cm^{-3}, and the electric field surged to approximately 300 mV/m. These observations suggest that the reconnection was initially in the plasma sheet, and then developed to involve lobe field lines. One may note that the ion bulk flow (depicted in Figure 1(b4)) in the LR does not exhibit a significant enhancement compared to PSR. This is probably due to that the ion velocity in this LR is underestimated due to a substantial portion of the high-energy ions were not measured by FPI, as shown in Figure 1(b7). The intervals of PSR and LR are differentiated by blue and orange shades, respectively.

Inflow regions for PSR and LR are observed at ~ 09:34 UT and ~ 09:42 UT (indicated in Figure 1b), respectively. Regardless of PSR or LR, the two inflow regions are

identified according to the criteria described in Section 3.1. However, in the LR inflow region, extremely low plasma density and nearly complete depletion of electron flux are observed compared to the inflow region of PSR. Here, we selected the interval from 04:21:26 UT (emergence of the outflow) to 04:34:20 UT (onset of T_e enhancement) to calculate the magnetic field fluctuation strength for PSR. The interval for LR spanned from 04:34:20 UT to 04:44:02 UT, corresponding to the increase and subsequent stabilization of T_e.

4. Statistical Study

We employed data from the MMS mission, following the outlined approach in Section 3, to investigate reconnection events in Earth's magnetotail from the year 2017 to 2020. Our objective is to elucidate the relationship between the fluctuation strength of these reconnections and various inflow parameters of reconnection, ambient plasma sheet fluctuation amplitude, upstream solar wind conditions, and geomagnetic activities. Note that the geomagnetic activities are treated as a consequence of reconnection, while the other parameters are regarded as causal factors for turbulent reconnection.

4.1 Criteria for Selecting Magnetotail Turbulent Reconnection Events and Calculation of Fluctuation Strength in Turbulent Reconnection

All the examined reconnection events are characterized by a tailward-to-earthward (or earthward-to-tailward) ion bulk flow reversal, concurrent with a corresponding reversal of B_z from negative to positive (or positive to negative). Interestingly, the power spectral densities (PSDs) of the magnetic field in all of these reconnections exhibit a power-law spectrum in the inertial range, which typically corresponds to frequencies below the ion cyclotron frequency (f_{ci}). The spectral indexes vary between -2.4 and -1.45, with an average of around -1.68. This is a common property of turbulent reconnection reported in previous observations (Eastwood et al., 2009; Huang et al., 2012; Ergun et al., 2018; Zhou et al., 2021). Recent numerical simulations find that magnetic reconnection is intrinsically an energy cascade process (Adhikari et al., 2020,

2021), so whether the formation of the power-law spectrum is a consequence of the development of turbulence in reconnection, or an intrinsic characteristic of reconnection is unclear.

We employed the following criteria to select the inflow region:

1. The interval should exhibit a large and stable $|B_X| > 10$ nT (Øieroset et al., 2023).

2. Density within this interval should be substantially lower than the surrounding region, accompanied by a significant reduction in differential energy flux of thermal electrons, usually above 1 keV.

3. The electric field within this interval should be relatively small (<10 mV/m) to avoid being in separatrix regions.

4. The period selected for the inflow region must not overlap with any segment of the outflow.

According to the above criteria, each reconnection event should have a corresponding inflow region. However, when a reconnection transits from PSR to LR, as exemplified in Section 3.2, corresponding inflow regions are expected in both types of reconnections. In fact, for most such events, the inflow region is observed exclusively in either the PSR or the LR region. Consequently, we select the period for calculating the fluctuation strength in the reconnection region, encompassing the outflow region and diffusion region, according to the following criteria: (1) For the PSR, selecting the time range for calculating fluctuation strengths is rather complex. If the reconnection event is similar to the one illustrated in Section 3.2 and the inflow region is found in the PSR, then the time range for calculating fluctuation strengths is chosen from the onset of the reconnection outflow to the beginning of the enhancement in T_e. If the PSR event is akin to the event presented in Section 3.1, then the time range is chosen from when the tailward flow (earthward flow) begins to appear until the earthward flow (tailward flow) nearly disappears. (2) If the inflow region is found in LR, the period for calculating fluctuation strength spans from the initiation of T_e increase to when T_e tends to be stabilized.

In this paper, we employ dB_{rec} and dE_{rec} to quantify the fluctuation strength in

reconnection. dB_{rec} and dE_{rec} are defined as $dB_{rec} = \sqrt{\sum_{i=x,y,z} \int_{0.05}^{f_{max}} P_{B,i} df}$ and $dE_{rec} = \sqrt{\sum_{i=x,y,z} \int_{0.05}^{f_{max}} P_{E,i} df}$, where $P_{B,i}$ and $P_{E,i}$ are the power spectral density of the ith component of the magnetic field and electric field, respectively; f_{max} represents the Nyquist frequency of the electromagnetic field data, which is 8 Hz for magnetic field **B** and 16 Hz for electric field **E**. The minimum frequency for integration is set to 0.05 Hz to eliminate the influence of large-scale current sheet flapping and coherent structures, such as flux ropes. Furthermore, the period corresponding to the inflow region is excluded in this calculation to focus on the turbulence in the outflow and diffusion region. Different from dB_{rec}, which represents electromagnetic fluctuations, dE_{rec} additionally involves electrostatic disturbances. If a certain parameter exhibits a weak correlation with dB_{rec} but a strong correlation with dE_{rec}, it indicates a possible dependency of that parameter on electrostatic disturbances.

According to the aforementioned criteria, a total of 31 reconnection events were selected from year 2017 to 2020. Figure 2 illustrates the distribution of these reconnection events in the X-Y plane of the geocentric solar magnetospheric (GSM) coordinates. Figure 2a shows that these events are approximately between -30 and -10 R_e in the X direction. Furthermore, 80% of events occurred on the dusk side, with only 20% located on the dawn side. This dawn-dusk asymmetric distribution of tail reconnection has been previously reported (Nagai et al.,2021; Lu et al., 2016) and is suggested to be caused by the Hall effect in the magnetotail current sheet (Lu et al., 2016). Figures 2b and 2c reveal that there is no clear dependence of dB_{rec} on the spatial position of these reconnection events.

4.2 The Influence of Inflow Parameters on Fluctuation Strength of Turbulent Reconnection

In the paper, we utilize both Spearman correlation coefficients (Scc) and Pearson correlation coefficient (Pcc) to assess the strength of the correlations between any two variables. The reason behind employing two different correlation coefficients lies in two considerations: (1) Pcc can assess the strength and direction of linear relationships

between two variables, while Scc can capture nonlinear monotonic correlations. In the case of non-perfect linearity, the use of Pcc may miss the monotonic information that Scc can reveal; (2) Pcc is highly sensitive to outliers, while Scc is less affected by anomalies, ensuring a more robust measure of correlation strength (Hauke et al., 2011; Schober et al., 2018). We refer to correlations with Scc or Pcc > 0.6 as good, 0.3< Scc or Pcc <0.6 as ambiguous, and Scc or Pcc < 0.3 as no correlation, the same definition as that used in Imada et al (2011).

Before performing statistical analysis, we validate the accuracy of the calculated inflow plasma parameters. In principle, the reconnection outflow speed increases as the increment of the inflow Alfvén speed ($V_{A,\,in}$) (Wu et al., 2011, 2012). Here we perform a correlation analysis between the inflow Alfven speed and the convective outflow speed. The outflow region is defined as the area where $|Vi_{\perp}| > 100$ km/s and $|B_x| < 10$ nT. Figure 3b shows the correlation between $V_{A,in}$, and electron convective outflow speed $Ve_{x\perp}$. We see that $Ve_{x\perp}$ is linearly correlated with $V_{A,in}$ as Pcc is close to 0.8, evidencing the reliability of the estimated inflow Alfven speed. Pcc between $V_{A,in}$, and ion convective speed $V_{ix\perp}$ is relatively poor partially because the ion bulk velocity is underestimated in some reconnection events. For example, the specific points, deviating from the overall trend, with higher $V_{A,\,in}$ but lower $V_{ix\perp}$ are observed in Figure 3a. We find that ion fluxes in these events typically exceed 10 keV, surpassing the measurement range of ion instruments (with an upper limit of 30 keV). Therefore, the main reason for the great difference between Scc ~ 0.8 and Pcc ~ 0.5 is the influence of these outliers. In conclusion, the good correlation between $V_{A,in}$, and outflow velocity validates the accuracy of the obtained inflow parameters.

Figure 4 illustrates the relationship between the fluctuation strength of reconnection and key inflow parameters $V_{A,in}$, β_{in}. Here LRs and PSRs are denoted by red and black squares, respectively. A good and robust correlation is observed between dB_{rec}, dE_{rec}, and $V_{A,in}$ (Scc > 0.6 and Pcc > 0.6). However, the correlation is not strictly linear as different dB_{rec} and dE_{rec} are corresponding to the same $V_{A,in}$. Notably, the correlation between dE_{rec} and $V_{A,in}$ (Scc ~ 0.75, Pcc ~ 0.79) is stronger than that between dB_{rec} and $V_{A,\,in}$ (Scc, Pcc ~ 0.62).

β_{in} exhibits a clear negative exponential correlation with dB_{rec} and dE_{rec} as shown in Figures 4b and 4d. In a logarithmic scale, the perturbation magnitude exhibits an almost linear relationship with β_{in}, with correlation coefficients of Pcc ~ -0.7 for dB_{rec} and Pcc ~ -0.8 for dE_{rec}. These correlation coefficients suggest a good correlation among the parameters. Similarly, these data points distribute along an exponential function over a broader range. In other words, under the same inflow parameters, there are additional factors further driving the evolution of reconnection towards turbulence. Moreover, LR events (red squares) typically have higher values of $V_{A,in,}$ and lower β_{in}. This suggests that as reconnection progresses into the lobe region, there is a discernible increase in the fluctuation amplitude of the electromagnetic field. In contrast, reconnection within the plasma sheet, constrained by the inflow parameters, may not undergo a highly turbulent evolution.

We next analyze the influence of the fluctuation amplitude in the inflow region to dB_{rec} and dE_{rec}. There is an obvious positive correlation between the inflow magnetic (dB_{in}) or electric (dE_{in}) field disturbance and dB_{rec} or dE_{rec} (Figures 5a and 5b). The fluctuation strength in the inflow region could be another crucial factor influencing turbulent reconnection. As depicted in Figure 5c, the pronounced positive correlation between dB_{in} and dE_{in} suggests that most fluctuations in the reconnection inflow region are electromagnetic in nature. Recent MMS observations reveal that the energy conversion rate J·E within the electron diffusion region (EDR) occasionally shows non-uniformity, featuring significant positive and negative peaks at electron scales (Burch et al., 2016, 2018; Cassak et al., 2017; Genestreti et al., 2017). Genestreti et al. (2022) uncover a positive correlation between the inhomogeneity of J·E and the directional change of the magnetic field in the inflow region, suggesting that the rapid variation of magnetic field direction in the inflow region may cause spatial non-uniformity at electron scales in the EDR. Motivated by their analysis, we investigate the relationship between the directional variations of the magnetic field in the inflow region $\langle \mathrm{acos}\,(\mathbf{B_{in}} \cdot \langle \mathbf{B_{in}} \rangle) \rangle$ and fluctuation strength in reconnection. The bracket $\langle \quad \rangle$ means time average, the same as Genestreti et al. (2022). As shown in Figure 5d, both Scc and Pcc are around -0.1, denoting no correlation. Consequently, the fluctuation strength

shows no dependence on the directional change of the inflow magnetic field.

In the following we examine the relationship between fluctuation strength in the pre-reconnection plasma sheet and that during reconnection to examine the contribution of the pre-existing fluctuations in the plasma sheet to the turbulence in reconnection. The pre-reconnection plasma sheet is identified as the region where $|V_{ix}|<100$ km/s, $|V_i|<200$ km/s, and Plasma $\beta > 0.5$. We see that both Scc and Pcc are less than 0.42 (Figures 5e and 5f), denoting ambiguous correlation, which implies that the electromagnetic disturbances in the plasma sheet before reconnection do not directly influence the fluctuation strength in reconnection. In other words, the observed turbulences during the reconnection process were primarily driven by reconnection rather than remnants of the pre-existing fluctuations in the ambient plasma sheet.

4.3 The Influence of Upstream Solar Wind Conditions on the Fluctuation Strength of Turbulent Reconnection

Previous studies indicate a time delay between changes in solar wind properties (including solar wind speed and dynamic pressure) and the interplanetary magnetic field (IMF), and the onset of a substorm, typically ranging from 20 to 60 minutes (Gérard et al., 2004; Liou et al., 1999; Meng et al., 1973). In this analysis, we calculate the average solar wind parameters in 1 hour immediately preceding the onset of reconnection and compare these parameters with the fluctuation strength of reconnection. Because unambiguously determining the exact onset time for reconnection in observation is extremely difficult, we refer to the onset of reconnection as the onset of reconnection outflow observed by MMS. Figure 6 illustrates that only the IMF cone angle, defined as $\cos^{-1}(B_y/|\mathbf{B}|)$, and solar wind dynamic pressure (P_{sw}) exhibit a certain correlation with the fluctuation strength. Figure 6b shows that the magnetic field fluctuation strength increases as the increment of the cone angle. Moreover, for all the LR events, the corresponding cone angles exceed 60°, and the corresponding clock angles surpass 120° or fall below -100°, which indicates a southward tilt of the IMF in LR events. On the other hand, fluctuation strength is not greater in association with a larger cone angle compared to a small cone angle for the

PSR events. The cone or clock angle corresponding to these PSR events is not concentrated in a specific angle range; Instead, they are distributed across various angles. A clear correlation between P_{sw} and dB_{rec} can be seen in Figure 6d. Notably, Pcc ~ 0.73 is much larger than Scc ~ 0.59. This disparity is likely because Pcc is inflated due to the existence of unusually large dB_{rec} and dynamic pressure events (Hauke et al., 2011; Schober et al., 2018). Anyway, the consistently positive correlation is a notable and robust observation. The ambiguous relationship between dE_{rec} and the cone angle and P_{sw} in Figures 6f and 6h implies that, unlike electromagnetic disturbances, there is no obvious dependence of the electrostatic disturbances on IMF cone angle and P_{sw}. In addition, Figures 6a and 6d demonstrate no dependency between (dB_{rec}, dE_{rec}) and the clock angle, with Scc and Pcc both below 0.2.

The temporal variation of the IMF may also impact the fluctuation strength. To quantify the temporal variations of the IMF, we assess the sum of variances of the three IMF components ($\sum_{i=x,y,z} Var(IMF\ B_i)$) within the one hour immediately preceding the reconnection. Figure 7 illustrates that the temporal variations of the IMF demonstrate no discernible correlation with electromagnetic disturbances during reconnection since both Scc and Pcc are less than 0.2.

4.4 The influence of the fluctuation strength of turbulent reconnection on geomagnetic activity

Below we analyze the relation between the strength of reconnection-driven turbulence and the intensity of magnetic storms and substorms. We employed average AL and SYM-H index during the observed reconnection interval to represent substorm and magnetic storm intensity for each event. We see that the fluctuation strength in reconnection does not exhibit a significant correlation with geomagnetic activity and the majority of reconnection events do not correspond to the occurrence of magnetic storms since the SYM-H index > -30 nT (Loewe & Prolss, 1997). There is an ambiguous negative correlation between (dE_{rec}, dB_{rec}) and AL index, where Scc ~ -0.5 and Pcc ~ -0.4 (Figure 8a), Scc~ -0.5 and Pcc~ -0.62 (Figure 8c). This suggests that tail reconnection with stronger electromagnetic fluctuation may contribute to a

larger substorm.

5. Discussion and Summary

We have investigated 31 reconnection events occurring in the Earth's magnetotail, corresponding to various inflow Alfvén speeds from 500 to 5000 km/s and β values ranging from 0.1 to 10. To gain insights into the principal factors that propel the evolution of reconnection into a turbulent state and the effects of these turbulent reconnections, we analyze the correlation of the reconnection inflow parameters, solar wind conditions, and geomagnetic activity with the fluctuation strength in reconnection.

We find a pronounced negative exponential correlation between β_{in} and (dB_{rec}, dE_{rec}). Specifically, as β_{in} decreases, the fluctuation strength increases. The positive correlation between $V_{A,in}$ and turbulent strength is also evident. Since LR is generally associated with larger $V_{A,in}$ and lower β_{in}, it is usually characterized by strong turbulence. Moreover, stronger turbulence can enhance energy conversion during reconnection (Jin et al., 2024), and may lead to particle heating and acceleration in LR (Oka et al., 2022). In contrast, PSR, characterized by smaller $V_{A,in}$ and higher β_{in}, tends to display smaller fluctuation strength, and end in a predominantly laminar flow state. This implies that, as reconnection progresses into the lobe region, there is a higher likelihood of driving large amplitude fluctuation. We should note that $V_{A,in}$ and β_{in} are not independent as they are connected by the inflow plasma density n_{in}. High $V_{A,in}$, and low β_{in} generally correspond to a small n_{in}, which results in a large energy gain per particle during reconnection (Phan et al., 2013). Accordingly, we suggest that higher-energy particles tend to excite instabilities with larger fluctuations, which leads to turbulent reconnection with stronger fluctuations.

One intriguing discovery is that dB_{in} is also correlated with dB_{rec}. It is essential to recognize that a correlation between dB_{in} and dB_{rec} does not necessarily mean a causal relationship between dB_{in} and dB_{rec}, as fluctuations in the inflow region may stem from the outflow region. There are two possible scenarios: (1) $V_{A,in,}$ and dB_{in} may independently be correlated with dB_{rec}. If this is the case, then we have an explanation

of why reconnection with similar $V_{A,in}$ and β_{in} corresponds to different fluctuation strengths as shown in Figure 4. This is because the electromagnetic fluctuations in the inflow region are another crucial factor driving the evolution of reconnection into turbulence. (2) dB_{in} is affected by dB_{rec} because the outflow fluctuation may somehow propagate into the inflow region (e.g., Lapenta et al., 2008).

Note that dB_{rec} is independent of $\langle \mathrm{acos}\,(\mathbf{B_{in}} \cdot \langle \mathbf{B_{in}} \rangle) \rangle$, which indicates that the variations of the inflow magnetic field direction do not affect the fluctuation strength during the reconnection. This result is distinct from the main conclusion of Genestreti et al. (2022), which shows that the time variability of the inflow magnetic field direction is best correlated with the standard deviation of the disturbance of energy conversion within EDR. However, Genestreti et al. (2022) only take into account the variability in the EDR whereas our study examines a broader reconnection region (including outflow region and diffusion region). Thus, the triggering factor of fluctuation in different regions may be distinct.

The correlation between the IMF cone angle and dB_{rec} means that a larger cone angle corresponds to a stronger fluctuation strength in turbulent reconnection. The clock angle for these strong turbulent events predominantly centers around ±120°. In other words, reconnection is more likely to develop into a turbulent state when the IMF is tilted southward. Scurry et al. (1994) found a positive correlation between the efficiency of magnetopause reconnection and the cone angle (Scurry et al., 1994). The increased efficiency of magnetopause reconnection may lead to the accumulation of a large amount of magnetic energy in the tail-lobe, increasing $V_{A,in}$, ultimately causing the reconnection in the magnetotail to evolve into a more turbulent state. In addition, observations have shown that the enhancement of P_{sw} further compresses the magnetosphere, leading to explosive reconnection in the magnetotail [Boudouridis et al., 2007; Connor et al., 2014]. In our statistical results, there is a clear positive correlation between P_{sw} and dB_{rec}, suggesting that when P_{sw} increases, the Earth's magnetotail is compressed and $|B_x|$ significantly increases in the lobe. This enhances the magnetic energy in the inflow region, which produces a larger outflow, finally promoting reconnection to become more turbulent.

Numerical simulations find that the guide field is probably a key parameter in controlling the fluctuation level in reconnection (Che et al., 2011; Daughton et al., 2011). Here we examine the connection between the guide field B_g and (dB_{rec}, dE_{rec}). Determining the magnitude of B_g bears large uncertainty (Borg et al., 2012). The out-of-plane magnetic field (B_y) in the electron diffusion regions (EDR) is a good measure of the magnitude of the guide field. This approach is widely adopted in observation to estimate the guide field strength (Torbert et al., 2018; Chen et al., 2019; Zhou et al., 2019). Three turbulent reconnection events with EDR observed by MMS were investigated to check whether these events exhibited a discernible relationship between B_g and dB_{rec}. We divide the average B_y within the EDR by the inflow magnetic field B_x to obtain the normalized guide field B_g. Our preliminary analyses find that for smaller B_g, dB_{rec} does not exhibit a clear correlation with B_g. For instance, in the July 11, 2017 event with $B_g \sim 0.04$, dB_{rec} is approximately 1.4 nT (Torbert et al., 2018), while in the August 27, 2018 event with $B_g \sim 0.1$, dB_{rec} is about 1.2 nT (Tang et al., 2022). However, a moderately large B_g may bring more intense magnetic field disturbances, as observed in the event of July 3, 2017, with $B_g \sim 0.3$ and dB_{rec} of 3.9 nT (Chen et al., 2019). Here we do not find a clear association between B_g and dB_{rec} because of the scarcity of the reconnection events in which the guide field strength can be reliably determined.

Previous studies have identified magnetotail reconnection as a primary driver of magnetospheric storms and substorms (Angelopoulos et al., 2008; Imber et al., 2011; Nagai & Machida, 1998). However, our results indicate a poor correlation between fluctuation strength and geomagnetic activity. Note that the SYM-H index is a manifestation of the ring current strength and the AL index is closely related to the field-aligned current (FAC), whereas reconnection is not directly linked to either of them. It has been suggested that bursty bulk flows generated by tail reconnection disrupt the cross-tail current in the flow-braking region around X ~ -10 Re, leading to the formation of FACs and consequently the creation of a substorm current wedge (Forsyth et al., 2008; Shiokawa et al., 1998; Yu et al., 2017). Moreover, the ring current is mainly carried by heated particles (Liemohn et al., 2000; Sato & Iijima, 1979). However, Jin et al. (2024) demonstrate that while stronger turbulence indeed enhances the conversion

of magnetic energy to plasma kinetic energy, it mainly increases the bulk flow energy while its impact on plasma heating is negligible. Cheng et al. (2013) find that the occurrence of FACs in the plasma sheet boundary layers increases monotonically with the IMF cone angle and peaks at clock angles of -90° and +110° (Cheng et al., 2013). Interestingly, the correlation between FACs and clock angle and cone angle is strikingly similar to that between (dB_{rec}, dE_{rec}) and these angles, which implies an underlying relationship between fluctuation strength and FAC, as illustrated in Figures 8a and 8c, with a correlation coefficient of about 0.5 between (dE_{rec}, dB_{rec}) and the AL index.

In summary, we have performed a statistical analysis related to the fluctuation strength (dE_{rec}, dB_{rec}) in magnetotail reconnection. Our main results are summarized below.

(1) There exists a notable positive correlation between the inflow Alfven speed $V_{A,in,}$ and fluctuation strength of reconnection, while β_{in} displays a distinct negative exponential correlation with fluctuation strength. We also notice a strong positive correlation between electromagnetic fluctuations in the inflow region and fluctuation strength, though the causality remains unclear. Therefore, inflow parameters are crucial factors influencing the fluctuation strength in reconnection.

(2) Regarding solar wind conditions, both the upstream IMF cone angle and solar wind dynamic pressure demonstrate a good positive correlation with fluctuation strength, whereas the IMF clock angle exhibits no correlation with fluctuation strength. LR events predominantly correspond to IMF clock angle of $\pm$120°. This may imply that, under enhanced solar wind pressure and southward IMF orientation, the heightened energy load in the tail lobe could potentially facilitate the generation of large-amplitude turbulence during reconnection.

(3) The fluctuation strength has an ambiguous relation with the AL index, while it has no dependency on the SYM-H index. In other words, the strength of fluctuation in reconnection does not directly impact the intensity of substorm and magnetic storm.

The relationship between turbulence and magnetic reconnection is inherently complex and involves the coupling of multi-scale processes. While this study examines

the primary factors influencing fluctuation strength within reconnection, the predominant instabilities causing turbulence remain elusive. The intrinsic limitations of observation prevent us from tracking the temporal evolution of turbulence during the reconnection process. Therefore, future studies are anticipated to combine in-situ satellite observations and numerical simulations to perform a deeper analysis of turbulent reconnection under different inflow conditions.

Acknowledgment

We extend our sincere appreciation to the entire MMS team for their invaluable contribution to high-quality, high-precision data, which was essential for the successful completion of this research endeavor. Furthermore, we acknowledge the financial support provided by the National Natural Science Foundation of China (NSFC) under grants No. 42130211, 42104156, 42074197, and 41774154, as well as the Natural Science Foundation of Jiangxi Province grant 20224BAB211021, which facilitated the execution of this study. All data utilized in this research were sourced from the MMS Scientific Data Center, accessible at https://lasp.colorado.edu/mms/sdc/public/. Additionally, we would like to express our gratitude for the availability of the SPEDAS software (Space Physics Environment Data Analysis Software), downloaded from http://spedas.org/blog/, which was instrumental in the creation of the figures presented in this work.

Reference

Adhikari, S., Shay, M. A., Parashar, T. N., Pyakurel, P. S., Matthaeus, W. H., Godzieba, D., et al. (2020). Reconnection from a turbulence perspective. Physics of Plasmas, 27(4), 042305. https://doi.org/10.1063/1.5128376

Adhikari, S., Parashar, T. N., Shay, M. A., Matthaeus, W. H., Pyakurel, P. S., Fordin, S., et al. (2021). Magnetic reconnection as an energy cascade process. Physical Review E, 104(6), 065206. https://doi.org/10.1103/PhysRevE.104.065206

Angelopoulos, V., McFadden, J. P., Larson, D., Carlson, C. W., Mende, S. B., Frey, H., et al. (2008). Tail Reconnection Triggering Substorm Onset. Science, 321(5891), 931–935. https://doi.org/10.1126/science.1160495

Bergstedt, K., Ji, H., Jara-Almonte, J., Yoo, J., Ergun, R. E., & Chen, L. -J. (2020). Statistical Properties of Magnetic Structures and Energy Dissipation during Turbulent Reconnection in the Earth's Magnetotail. Geophysical Research Letters, 47(19).

https://doi.org/10.1029/2020GL088540
Borg, A. L., Taylor, M. G. G. T., & Eastwood, J. P. (2012). Observations of magnetic flux ropes during magnetic reconnection in the Earth's magnetotail. Annales Geophysicae, 30(5), 761–773. https://doi.org/10.5194/angeo-30-761-2012
Boudouridis, A., Lyons, L. R., Zesta, E., & Ruohoniemi, J. M. (2007). Dayside reconnection enhancement resulting from a solar wind dynamic pressure increase: PRESSURE-INDUCED DAYSIDE RECONNECTION. Journal of Geophysical Research: Space Physics, 112(A6), n/a-n/a. https://doi.org/10.1029/2006JA012141
Burch, J. L., Torbert, R. B., Phan, T. D., Chen, L.-J., Moore, T. E., Ergun, R. E., et al. (2016). Electron-scale measurements of magnetic reconnection in space. PLASMA ASTROPHYSICS, 352(6290), aaf2939. https://doi.org/10.1126/science.aaf2939
Burch, J. L., Ergun, R. E., Cassak, P. A., Webster, J. M., Torbert, R. B., Giles, B. L., et al. (2018). Localized Oscillatory Energy Conversion in Magnetopause Reconnection. Geophysical Research Letters, 45(3), 1237–1245. https://doi.org/10.1002/2017GL076809
Cassak, P. A., Genestreti, K. J., Burch, J. L., Phan, T. -D., Shay, M. A., Swisdak, M., et al. (2017). The Effect of a Guide Field on Local Energy Conversion During Asymmetric Magnetic Reconnection: Particle-in-Cell Simulations. Journal of Geophysical Research: Space Physics, 122(11). https://doi.org/10.1002/2017JA024555
Chaston, C. C., Johnson, J. R., Wilber, M., Acuna, M., Goldstein, M. L., & Reme, H. (2009). Kinetic Alfvén Wave Turbulence and Transport through a Reconnection Diffusion Region. Physical Review Letters, 102(1), 015001. https://doi.org/10.1103/PhysRevLett.102.015001
Che, H., Drake, J. F., Swisdak, M., & Yoon, P. H. (2010). Electron holes and heating in the reconnection dissipation region: ELECTRON HOLES AND HEATING IN RECONNECTION. Geophysical Research Letters, 37(11), n/a-n/a. https://doi.org/10.1029/2010GL043608
Che, H., Drake, J. F., & Swisdak, M. (2011). A current filamentation mechanism for breaking magnetic field lines during reconnection. Nature, 474(7350), 184–187. https://doi.org/10.1038/nature10091
Chen, L. -J., Wang, S., Hesse, M., Ergun, R. E., Moore, T., Giles, B., et al. (2019). Electron Diffusion Regions in Magnetotail Reconnection Under Varying Guide Fields. Geophysical Research Letters, 46(12), 6230–6238. https://doi.org/10.1029/2019GL082393
Cheng, Z. W., Shi, J. K., Dunlop, M., & Liu, Z. X. (2013). Influences of the interplanetary magnetic field clock angle and cone angle on the field-aligned currents in the magnetotail. Geophysical Research Letters, 40(20), 5355–5359. https://doi.org/10.1002/2013GL056737
Connor, H. K., Zesta, E., Ober, D. M., & Raeder, J. (2014). The relation between transpolar potential and reconnection rates during sudden enhancement of solar wind dynamic pressure: OpenGGCM-CTIM results: Relation between CPCP and reconnection. Journal of Geophysical Research: Space Physics, 119(5), 3411–3429. https://doi.org/10.1002/2013JA019728
Daughton, W., Roytershteyn, V., Karimabadi, H., Yin, L., Albright, B. J., Bergen, B., & Bowers, K. J. (2011). Role of electron physics in the development of turbulent magnetic reconnection in collisionless plasmas. Nature Physics, 7(7), 539–542. https://doi.org/10.1038/nphys1965
Divin, A., Khotyaintsev, Yu. V., Vaivads, A., André, M., Markidis, S., & Lapenta, G. (2015). Evolution of the lower hybrid drift instability at reconnection jet front. Journal of Geophysical Research: Space Physics, 120(4), 2675–2690. https://doi.org/10.1002/2014JA020503
Eastwood, J. P., Phan, T. D., Bale, S. D., & Tjulin, A. (2009). Observations of Turbulence Generated

609 by Magnetic Reconnection. Physical Review Letters, 102(3), 035001.
610 https://doi.org/10.1103/PhysRevLett.102.035001
611 Ergun, R. E., Tucker, S., Westfall, J., Goodrich, K. A., Malaspina, D. M., Summers, D., et al. (2016).
612 The Axial Double Probe and Fields Signal Processing for the MMS Mission. Space Science
613 Reviews, 199(1–4), 167–188. https://doi.org/10.1007/s11214-014-0115-x
614 Ergun, R. E., Goodrich, K. A., Wilder, F. D., Ahmadi, N., Holmes, J. C., Eriksson, S., et al. (2018).
615 Magnetic Reconnection, Turbulence, and Particle Acceleration: Observations in the Earth's
616 Magnetotail. Geophysical Research Letters, 45(8), 3338–3347.
617 https://doi.org/10.1002/2018GL076993
618 Ergun, R. E., Ahmadi, N., Kromyda, L., Schwartz, S. J., Chasapis, A., Hoilijoki, S., et al. (2020).
619 Particle Acceleration in Strong Turbulence in the Earth's Magnetotail. The Astrophysical Journal,
620 898(2), 153. https://doi.org/10.3847/1538-4357/ab9ab5
621 Ergun, R. E., Pathak, N., Usanova, M. E., Qi, Y., Vo, T., Burch, J. L., et al. (2022). Observation of
622 Magnetic Reconnection in a Region of Strong Turbulence. The Astrophysical Journal Letters,
623 935(1), L8. https://doi.org/10.3847/2041-8213/ac81d4
624 Forsyth, C., Lester, M., Cowley, S. W. H., Dandouras, I., Fazakerley, A. N., Fear, R. C., et al. (2008).
625 Observed tail current systems associated with bursty bulk flows and auroral streamers during a
626 period of multiple substorms. Annales Geophysicae, 26(1), 167–184.
627 https://doi.org/10.5194/angeo-26-167-2008
628 Fu, H. S., Vaivads, A., Khotyaintsev, Y. V., André, M., Cao, J. B., Olshevsky, V., et al. (2017).
629 Intermittent energy dissipation by turbulent reconnection: DISSIPATION BY TURBULENT
630 RECONNECTION. Geophysical Research Letters, 44(1), 37–43.
631 https://doi.org/10.1002/2016GL071787
632 Genestreti, K. J., Burch, J. L., Cassak, P. A., Torbert, R. B., Ergun, R. E., Varsani, A., et al. (2017).
633 The Effect of a Guide Field on Local Energy Conversion During Asymmetric Magnetic
634 Reconnection: MMS Observations. Journal of Geophysical Research: Space Physics, 122(11).
635 https://doi.org/10.1002/2017JA024247
636 Genestreti, Kevin J., Li, X., Liu, Y.-H., Burch, J. L., Torbert, R. B., Fuselier, S. A., et al. (2022). On
637 the origin of "patchy" energy conversion in electron diffusion regions. Physics of Plasmas, 29(8),
638 082107. https://doi.org/10.1063/5.0090275
639 Gérard, J. -C., Hubert, B., Grard, A., Meurant, M., & Mende, S. B. (2004). Solar wind control of
640 auroral substorm onset locations observed with the IMAGE-FUV imagers. Journal of
641 Geophysical Research: Space Physics, 109(A3), 2003JA010129.
642 https://doi.org/10.1029/2003JA010129
643 Gershman, D. J., Avanov, L. A., Boardsen, S. A., Dorelli, J. C., Gliese, U., Barrie, A. C., et al. (2017).
644 Spacecraft and Instrument Photoelectrons Measured by the Dual Electron Spectrometers on MMS.
645 Journal of Geophysical Research: Space Physics, 122(11).
646 https://doi.org/10.1002/2017JA024518
647 Gershman, D. J., Dorelli, J. C., Avanov, L. A., Gliese, U., Barrie, A., Schiff, C., et al. (2019).
648 Systematic Uncertainties in Plasma Parameters Reported by the Fast Plasma Investigation on
649 NASA's Magnetospheric Multiscale Mission. Journal of Geophysical Research: Space Physics,
650 124(12), 10345–10359. https://doi.org/10.1029/2019JA026980
651 Hauke, J., & Kossowski, T. (2011). Comparison of Values of Pearson's and Spearman's Correlation
652 Coefficients on the Same Sets of Data. QUAGEO, 30(2), 87–93. https://doi.org/10.2478/v10117-

011-0021-1
Huang, S. Y., Zhou, M., Sahraoui, F., Deng, X. H., Pang, Y., Yuan, Z. G., et al. (2010). Wave properties in the magnetic reconnection diffusion region with high β : Application of the k - filtering method to Cluster multispacecraft data: WAVES IN RECONNECTION REGION. Journal of Geophysical Research: Space Physics, 115(A12), n/a-n/a. https://doi.org/10.1029/2010JA015335
Huang, S. Y., Zhou, M., Sahraoui, F., Vaivads, A., Deng, X. H., André, M., et al. (2012). Observations of turbulence within reconnection jet in the presence of guide field: TURBULENCE IN THE RECONNECTION JET. Geophysical Research Letters, 39(11), n/a-n/a. https://doi.org/10.1029/2012GL052210
Huang, S. Y., Zhang, J., Yuan, Z. G., Jiang, K., Wei, Y. Y., Xu, S. B., et al. (2022). Intermittent Dissipation at Kinetic Scales in the Turbulent Reconnection Outflow. Geophysical Research Letters, 49(1). https://doi.org/10.1029/2021GL096403
Imada, S., Hirai, M., Hoshino, M., & Mukai, T. (2011). Favorable conditions for energetic electron acceleration during magnetic reconnection in the Earth's magnetotail: FAVORABLE CONDITIONS FOR ACCELERATION. Journal of Geophysical Research: Space Physics, 116(A8), n/a-n/a. https://doi.org/10.1029/2011JA016576
Imber, S. M., Slavin, J. A., Auster, H. U., & Angelopoulos, V. (2011). A THEMIS survey of flux ropes and traveling compression regions: Location of the near-Earth reconnection site during solar minimum: TAIL RECONNECTION DURING SOLAR MINIMUM. Journal of Geophysical Research: Space Physics, 116(A2), n/a-n/a. https://doi.org/10.1029/2010JA016026
Jin, R., Zhou, M., Pang, Y., Deng, X., & Yi, Y. (2022). Characteristics of Turbulence Driven by Transient Magnetic Reconnection in the Terrestrial Magnetotail. The Astrophysical Journal, 925(1), 17. https://doi.org/10.3847/1538-4357/ac390c
Jin, R., Zhou, M., Yi, Y., Man, H., Zhong, Z., Pang, Y., & Deng, X. (2024). Enhanced Energy Conversion by Turbulence in Collisionless Magnetic Reconnection. The Astrophysical Journal, 965(1), 71. https://doi.org/10.3847/1538-4357/ad2841
Khotyaintsev, Yu. V., Graham, D. B., Steinvall, K., Alm, L., Vaivads, A., Johlander, A., et al. (2020). Electron Heating by Debye-Scale Turbulence in Guide-Field Reconnection. Physical Review Letters, 124(4), 045101. https://doi.org/10.1103/PhysRevLett.124.045101
Lapenta, G., Pucci, F., Goldman, M. V., & Newman, D. L. (2020). Local Regimes of Turbulence in 3D Magnetic Reconnection. The Astrophysical Journal, 888(2), 104. https://doi.org/10.3847/1538-4357/ab5a86
Lapenta, Giovanni. (2008). Self-Feeding Turbulent Magnetic Reconnection on Macroscopic Scales. Physical Review Letters, 100(23), 235001. https://doi.org/10.1103/PhysRevLett.100.235001
Lapenta, Giovanni, & Bettarini, L. (2011). Self-consistent seeding of the interchange instability in dipolarization fronts: KINK AND INTERCHANGE DURING DIPOLARIZATION. Geophysical Research Letters, 38(11), n/a-n/a. https://doi.org/10.1029/2011GL047742
Lapenta, Giovanni, Markidis, S., Goldman, M. V., & Newman, D. L. (2015). Secondary reconnection sites in reconnection-generated flux ropes and reconnection fronts. Nature Physics, 11(8), 690–695. https://doi.org/10.1038/nphys3406
Lapenta, Giovanni, Pucci, F., Olshevsky, V., Servidio, S., Sorriso-Valvo, L., Newman, D. L., & Goldman, M. V. (2018). Nonlinear waves and instabilities leading to secondary reconnection in reconnection outflows. Journal of Plasma Physics, 84(1), 715840103.

https://doi.org/10.1017/S002237781800003X
Lazarian, A., & Vishniac, E. T. (1999). Reconnection in a Weakly Stochastic Field. The Astrophysical Journal, 517(2), 700–718. https://doi.org/10.1086/307233
Li, X., Wang, R., Huang, C., Lu, Q., Lu, S., Burch, J. L., & Wang, S. (2022). Energy Conversion and Partition in Plasma Turbulence Driven by Magnetotail Reconnection. The Astrophysical Journal, 936(1), 34. https://doi.org/10.3847/1538-4357/ac84d7
Liemohn, M. W., Kozyra, J. U., Richards, P. G., Khazanov, G. V., Buonsanto, M. J., & Jordanova, V. K. (2000). Ring current heating of the thermal electrons at solar maximum. Journal of Geophysical Research: Space Physics, 105(A12), 27767–27776. https://doi.org/10.1029/2000JA000088
Lindqvist, P.-A., Olsson, G., Torbert, R. B., King, B., Granoff, M., Rau, D., et al. (2016). The Spin-Plane Double Probe Electric Field Instrument for MMS. Space Science Reviews, 199(1–4), 137–165. https://doi.org/10.1007/s11214-014-0116-9
Liou, K., Meng, C. -I, Lui, T. Y., Newell, P. T., Brittnacher, M., Parks, G., et al. (1999). On relative timing in substorm onset signatures. Journal of Geophysical Research: Space Physics, 104(A10), 22807–22817. https://doi.org/10.1029/1999JA900206
Loewe, C. A., & Prölss, G. W. (1997). Classification and mean behavior of magnetic storms. Journal of Geophysical Research: Space Physics, 102(A7), 14209–14213. https://doi.org/10.1029/96JA04020
Lu, S., Lin, Y., Angelopoulos, V., Artemyev, A. V., Pritchett, P. L., Lu, Q., & Wang, X. Y. (2016). Hall effect control of magnetotail dawn-dusk asymmetry: A three-dimensional global hybrid simulation. Journal of Geophysical Research: Space Physics, 121(12). https://doi.org/10.1002/2016JA023325
Lu, S., Lu, Q., Wang, R., Li, X., Gao, X., Huang, K., et al. (2023). Kinetic Scale Magnetic Reconnection with a Turbulent Forcing: Particle-in-cell Simulations. The Astrophysical Journal, 943(2), 100. https://doi.org/10.3847/1538-4357/acaf7a
Meng, C.-I., Tsurutani, B., Kawasaki, K., & Akasofu, S.-I. (1973). Cross-correlation analysis of the AE index and the interplanetary magnetic field B_z component. Journal of Geophysical Research, 78(4), 617–629. https://doi.org/10.1029/JA078i004p00617
Nagai, T., Fujimoto, M., Saito, Y., Machida, S., Terasawa, T., Nakamura, R., et al. (1998). Structure and dynamics of magnetic reconnection for substorm onsets with Geotail observations. Journal of Geophysical Research: Space Physics, 103(A3), 4419–4440. https://doi.org/10.1029/97JA02190
Nagai, Tsugunobu, & Shinohara, I. (2021). Dawn-Dusk Confinement of Magnetic Reconnection Site in the Near-Earth Magnetotail and Its Implication for Dipolarization and Substorm Current System. Journal of Geophysical Research: Space Physics, 126(11), e2021JA029691. https://doi.org/10.1029/2021JA029691
Øieroset, M., Phan, T. D., Oka, M., Drake, J. F., Fuselier, S. A., Gershman, D. J., et al. (2023). Scaling of Magnetic Reconnection Electron Bulk Heating in the High-Alfvén-speed and Low-β Regime of Earth's Magnetotail. The Astrophysical Journal, 954(2), 118. https://doi.org/10.3847/1538-4357/acdf44
Oka, M., Phan, T. D., Øieroset, M., Turner, D. L., Drake, J. F., Li, X., et al. (2022). Electron energization and thermal to non-thermal energy partition during earth's magnetotail reconnection. Physics of Plasmas, 29(5), 052904. https://doi.org/10.1063/5.0085647

Osman, K. T., Matthaeus, W. H., Gosling, J. T., Greco, A., Servidio, S., Hnat, B., et al. (2014). Magnetic Reconnection and Intermittent Turbulence in the Solar Wind. Physical Review Letters, 112(21), 215002. https://doi.org/10.1103/PhysRevLett.112.215002

Osman, K. T., Kiyani, K. H., Matthaeus, W. H., Hnat, B., Chapman, S. C., & Khotyaintsev, Yu. V. (2015). MULTI-SPACECRAFT MEASUREMENT OF TURBULENCE WITHIN A MAGNETIC RECONNECTION JET. The Astrophysical Journal, 815(2), L24. https://doi.org/10.1088/2041-8205/815/2/L24

Parker, E. N. (1957). Sweet's mechanism for merging magnetic fields in conducting fluids. Journal of Geophysical Research, 62(4), 509–520. https://doi.org/10.1029/JZ062i004p00509

Phan, T. D., Shay, M. A., Gosling, J. T., Fujimoto, M., Drake, J. F., Paschmann, G., et al. (2013). Electron bulk heating in magnetic reconnection at Earth's magnetopause: Dependence on the inflow Alfvén speed and magnetic shear. Geophysical Research Letters, 40(17), 4475–4480. https://doi.org/10.1002/grl.50917

Pollock, C., Moore, T., Jacques, A., Burch, J., Gliese, U., Saito, Y., et al. (2016). Fast Plasma Investigation for Magnetospheric Multiscale. Space Science Reviews, 199(1–4), 331–406. https://doi.org/10.1007/s11214-016-0245-4

Price, L., Swisdak, M., Drake, J. F., Cassak, P. A., Dahlin, J. T., & Ergun, R. E. (2016). The effects of turbulence on three-dimensional magnetic reconnection at the magnetopause. Geophysical Research Letters, 43(12), 6020–6027. https://doi.org/10.1002/2016GL069578

Price, L., Swisdak, M., Drake, J. F., Burch, J. L., Cassak, P. A., & Ergun, R. E. (2017). Turbulence in Three-Dimensional Simulations of Magnetopause Reconnection. Journal of Geophysical Research: Space Physics, 122(11). https://doi.org/10.1002/2017JA024227

Pucci, F., Servidio, S., Sorriso-Valvo, L., Olshevsky, V., Matthaeus, W. H., Malara, F., et al. (2017). Properties of Turbulence in the Reconnection Exhaust: Numerical Simulations Compared with Observations. The Astrophysical Journal, 841(1), 60. https://doi.org/10.3847/1538-4357/aa704f

Retinò, A., Sundkvist, D., Vaivads, A., Mozer, F., André, M., & Owen, C. J. (2007). In situ evidence of magnetic reconnection in turbulent plasma. Nature Physics, 3(4), 235–238. https://doi.org/10.1038/nphys574

Russell, C. T., Anderson, B. J., Baumjohann, W., Bromund, K. R., Dearborn, D., Fischer, D., et al. (2016). The Magnetospheric Multiscale Magnetometers. Space Science Reviews, 199(1–4), 189–256. https://doi.org/10.1007/s11214-014-0057-3

Sato, T., & Iijima, T. (1979). Primary sources of large-scale Birkeland currents. Space Science Reviews, 24(3). https://doi.org/10.1007/BF00212423

Schindler, K., Hesse, M., & Birn, J. (1988). General magnetic reconnection, parallel electric fields, and helicity. Journal of Geophysical Research, 93(A6), 5547. https://doi.org/10.1029/JA093iA06p05547

Schober, P., Boer, C., & Schwarte, L. A. (2018). Correlation Coefficients: Appropriate Use and Interpretation, 126(5).

Scurry, L., Russell, C. T., & Gosling, J. T. (1994). Geomagnetic activity and the beta dependence of the dayside reconnection rate. Journal of Geophysical Research: Space Physics, 99(A8), 14811–14814. https://doi.org/10.1029/94JA00794

Shiokawa, K., Baumjohann, W., Haerendel, G., Paschmann, G., Fennell, J. F., Friis-Christensen, E., et al. (1998). High-speed ion flow, substorm current wedge, and multiple Pi 2 pulsations. Journal of Geophysical Research: Space Physics, 103(A3), 4491–4507.

https://doi.org/10.1029/97JA01680
Sonnerup, B. U. Ö. (1984). Magnetic field reconnection at the magnetopause: An overview. In E. W. Hones (Ed.), Geophysical Monograph Series (Vol. 30, pp. 92–103). Washington, D. C.: American Geophysical Union. https://doi.org/10.1029/GM030p0092
Sun, H., Yang, Y., Lu, Q., Lu, S., Wan, M., & Wang, R. (2022). Physical Regimes of Two-dimensional MHD Turbulent Reconnection in Different Lundquist Numbers. The Astrophysical Journal, 926(1), 97. https://doi.org/10.3847/1538-4357/ac4158
Sundkvist, D., Retinò, A., Vaivads, A., & Bale, S. D. (2007). Dissipation in Turbulent Plasma due to Reconnection in Thin Current Sheets. Physical Review Letters, 99(2), 025004. https://doi.org/10.1103/PhysRevLett.99.025004
Tang, B. -B., Li, W. Y., Khotyaintsev, Yu. V., Graham, D. B., Gao, C. H., Chen, Z. Z., et al. (2022). Fine Structures of the Electron Current Sheet in Magnetotail Guide-Field Reconnection. Geophysical Research Letters, 49(9). https://doi.org/10.1029/2021GL097573
Torbert, R. B., Russell, C. T., Magnes, W., Ergun, R. E., Lindqvist, P.-A., LeContel, O., et al. (2016). The FIELDS Instrument Suite on MMS: Scientific Objectives, Measurements, and Data Products. Space Science Reviews, 199(1–4), 105–135. https://doi.org/10.1007/s11214-014-0109-8
Torbert, R. B., Burch, J. L., Phan, T. D., Hesse, M., Argall, M. R., Shuster, J., et al. (2018). Electron-scale dynamics of the diffusion region during symmetric magnetic reconnection in space. Science, 362(6421), 1391–1395. https://doi.org/10.1126/science.aat2998
Vörös, Z., Sasunov, Y. L., Semenov, V. S., Zaqarashvili, T. V., Bruno, R., & Khodachenko, M. (2014). RECONNECTION OUTFLOW GENERATED TURBULENCE IN THE SOLAR WIND. The Astrophysical Journal, 797(1), L10. https://doi.org/10.1088/2041-8205/797/1/L10
Wang, R., Wang, S., Lu, Q., Li, X., Lu, S., & Gonzalez, W. (2022). Direct observation of turbulent magnetic reconnection in the solar wind. Nature Astronomy, 7(1), 18–28. https://doi.org/10.1038/s41550-022-01818-5
Wu, P., & Shay, M. A. (2012). Magnetotail dipolarization front and associated ion reflection: Particle-in-cell simulations. Geophysical Research Letters, 39(8), 2012GL051486. https://doi.org/10.1029/2012GL051486
Wu, P., Shay, M. A., Phan, T. D., Oieroset, M., & Oka, M. (2011). Effect of inflow density on ion diffusion region of magnetic reconnection: Particle-in-cell simulations. Physics of Plasmas, 18(11), 111204. https://doi.org/10.1063/1.3641964
Yin, L., Daughton, W., Karimabadi, H., Albright, B. J., Bowers, K. J., & Margulies, J. (2008). Three-Dimensional Dynamics of Collisionless Magnetic Reconnection in Large-Scale Pair Plasmas. Physical Review Letters, 101(12), 125001. https://doi.org/10.1103/PhysRevLett.101.125001
Yoon, P. H., Rhee, T., & Ryu, C.-M. (2005). Self-Consistent Generation of Superthermal Electrons by Beam-Plasma Interaction. Physical Review Letters, 95(21), 215003. https://doi.org/10.1103/PhysRevLett.95.215003
Yu, Y., Cao, J., Fu, H., Lu, H., & Yao, Z. (2017). The effects of bursty bulk flows on global-scale current systems. Journal of Geophysical Research: Space Physics, 122(6), 6139–6149. https://doi.org/10.1002/2017JA024168
Zhong, Z. H., Tang, R. X., Zhou, M., Deng, X. H., Pang, Y., Paterson, W. R., et al. (2018). Evidence for Secondary Flux Rope Generated by the Electron Kelvin-Helmholtz Instability in a Magnetic Reconnection Diffusion Region. Physical Review Letters, 120(7), 075101. https://doi.org/10.1103/PhysRevLett.120.075101

Zhong, Z. H., Zhou, M., Deng, X. H., Song, L. J., Graham, D. B., Tang, R. X., et al. (2021). Three-Dimensional Electron-Scale Magnetic Reconnection in Earth's Magnetosphere. Geophysical Research Letters, 48(1), 2020GL090946. https://doi.org/10.1029/2020GL090946

Zhou, M., Deng, X. H., Li, S. Y., Pang, Y., Vaivads, A., Rème, H., et al. (2009). Observation of waves near lower hybrid frequency in the reconnection region with thin current sheet: LOWER HYBRID WAVES WITH RECONNECTION. Journal of Geophysical Research: Space Physics, 114(A2), n/a-n/a. https://doi.org/10.1029/2008JA013427

Zhou, M., Deng, X. H., Zhong, Z. H., Pang, Y., Tang, R. X., El-Alaoui, M., et al. (2019a). Observations of an Electron Diffusion Region in Symmetric Reconnection with Weak Guide Field. The Astrophysical Journal, 870(1), 34. https://doi.org/10.3847/1538-4357/aaf16f

Zhou, M., Deng, X. H., Zhong, Z. H., Pang, Y., Tang, R. X., El-Alaoui, M., et al. (2019b). Observations of an Electron Diffusion Region in Symmetric Reconnection with Weak Guide Field. The Astrophysical Journal, 870(1), 34. https://doi.org/10.3847/1538-4357/aaf16f

Zhou, M., Man, H. Y., Deng, X. H., Pang, Y., Khotyaintsev, Y., Lapenta, G., et al. (2021). Observations of Secondary Magnetic Reconnection in the Turbulent Reconnection Outflow. Geophysical Research Letters, 48(4), e2020GL091215. https://doi.org/10.1029/2020GL091215

Zhou, Meng, Ashour-Abdalla, M., Deng, X., Schriver, D., El-Alaoui, M., & Pang, Y. (2009). THEMIS observation of multiple dipolarization fronts and associated wave characteristics in the near-Earth magnetotail. Geophysical Research Letters, 36(20), L20107. https://doi.org/10.1029/2009GL040663

Figure 1

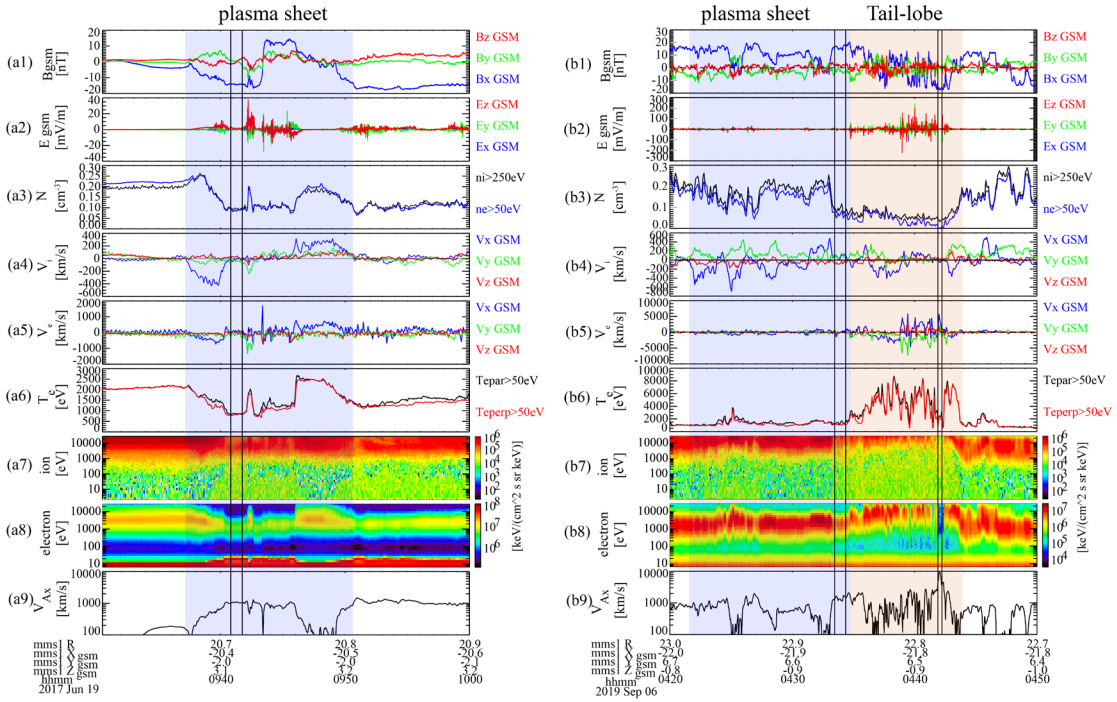

Figure 1. Overview of the turbulent reconnections: 19 June 2017 and 06 September

2019. From the top to bottom are: (a1, b1) three components of the magnetic field; (a2, b2) the electric field; (a3, b3) electron and ion number density; (a4, b4) three components of the ion bulk velocity and (a5, b5) electron bulk velocity; (a6, b6) electron parallel and perpendicular temperature; (a7, b7) ion and (a8, b8) electron differential energy fluxes; (a9, b9) the x component of the Alfven velocity. Here the ion and electron moment data are partial moment data with energy greater than 250 eV for ions and 50 eV for electrons. The PSR and LR regimes are highlighted in blue and orange, respectively. The black vertical lines indicate the inflow regions.

Figure 2

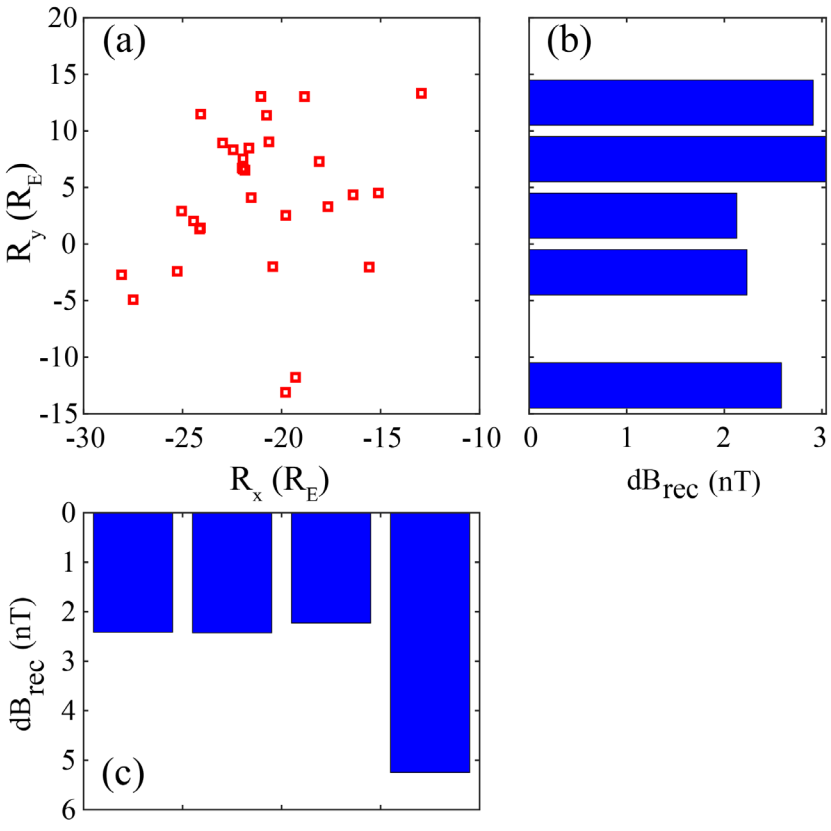

Figure 2. (a) Spatial distribution of turbulent reconnections in the GSM x-y plane; Distribution of dB_{rec} concerning position (b) R_y and (c) R_x.

Figure 3

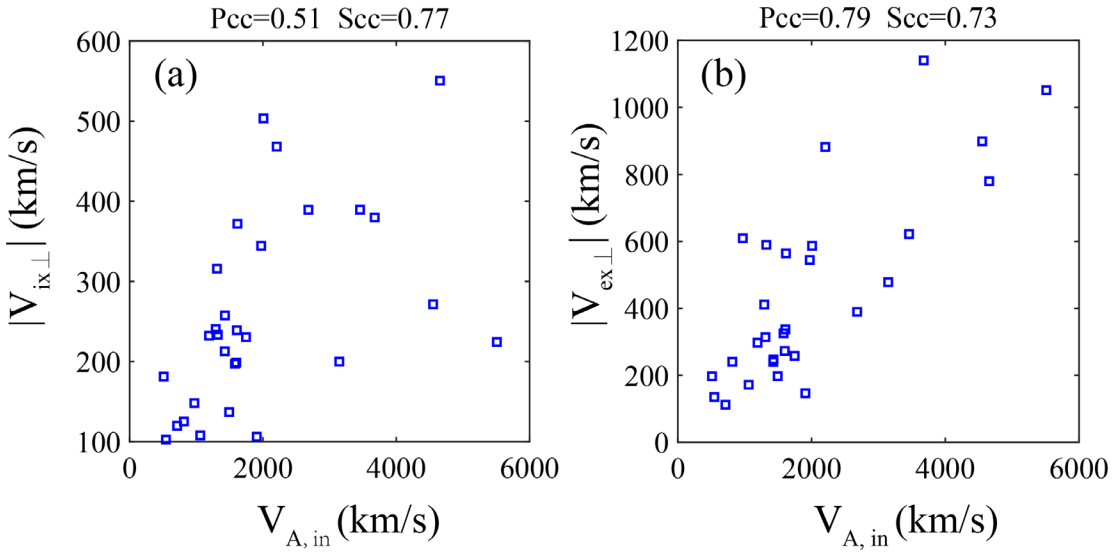

Figure 3. Correlation between the inflow Alfven speed and (a) the outflow ion convective speed $Vi_{x\perp}$ and (b) the outflow electrons convective speed $Vex_{\perp}$. "Scc" and "Pcc" at the top of each panel represent Spearman and Pearson correlation coefficients, respectively.

Figure 4

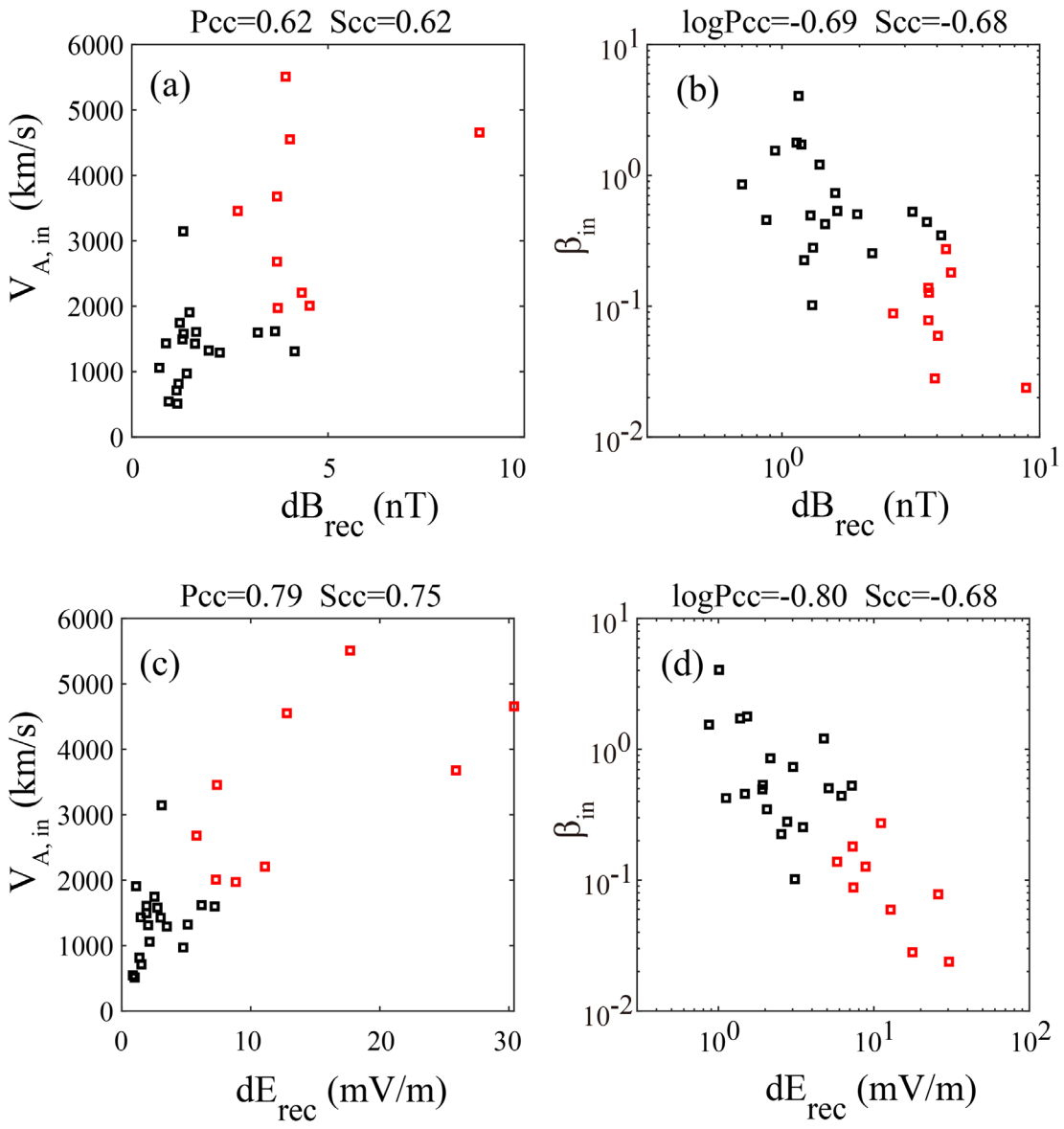

879

880 **Figure 4.** Scatter plot of the relationship between fluctuation strength dB_{rec} (a,b), dE_{rec}
881 (c,d) for the turbulent reconnections versus (a, c) inflow Alfven speed $V_{A,in}$ and (b, d)
882 inflow β_{in}. The red squares represent LRs and the black squares represent PSRs..

883

884 **Figure 5**

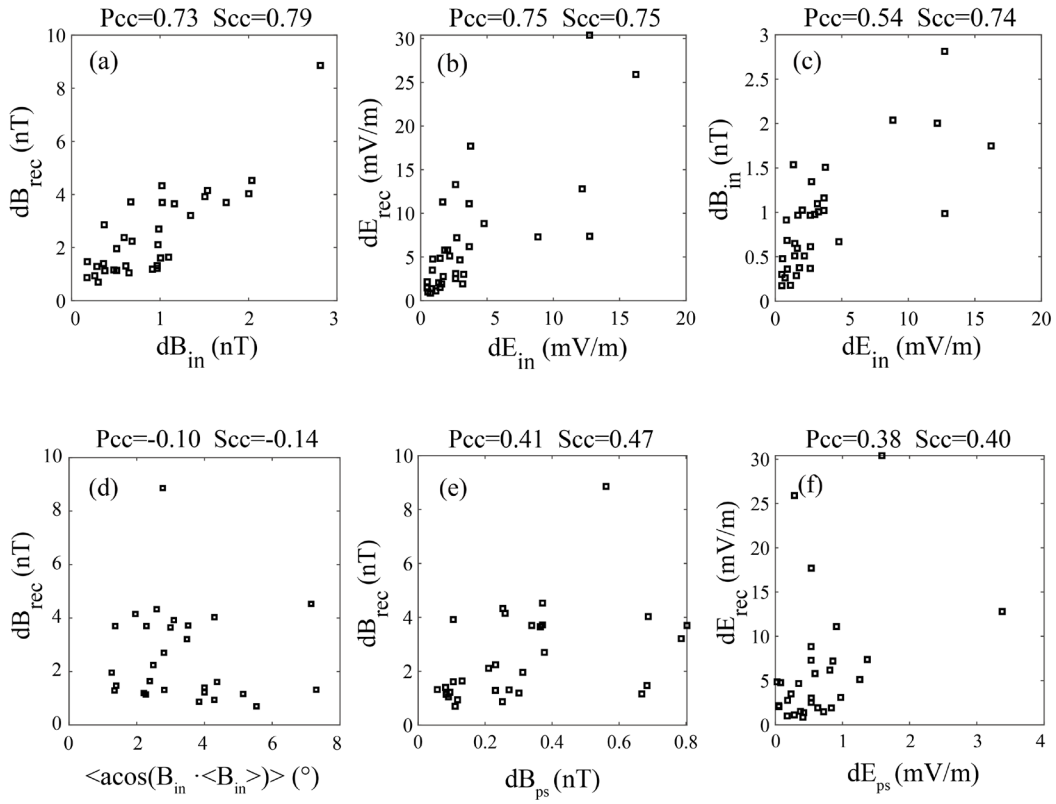

Figure 5. (a) Correlation between dB_{rec} and dB_{in}, and (b) correlation between dE_{rec} and dE_{in}; (c) dE_{in} VS dB_{in}; (d) correlation between the temporal variations of the magnetic field in the inflow region $\langle \mathrm{acos}\,(\mathbf{B_{in}} \cdot \langle \mathbf{B_{in}} \rangle) \rangle$ and dB_{rec}; (e) fluctuation strength in the plasma sheet region before reconnection dB_{ps} VS dB_{rec}; (f) dE_{ps} VS dE_{rec}.

Figure 6

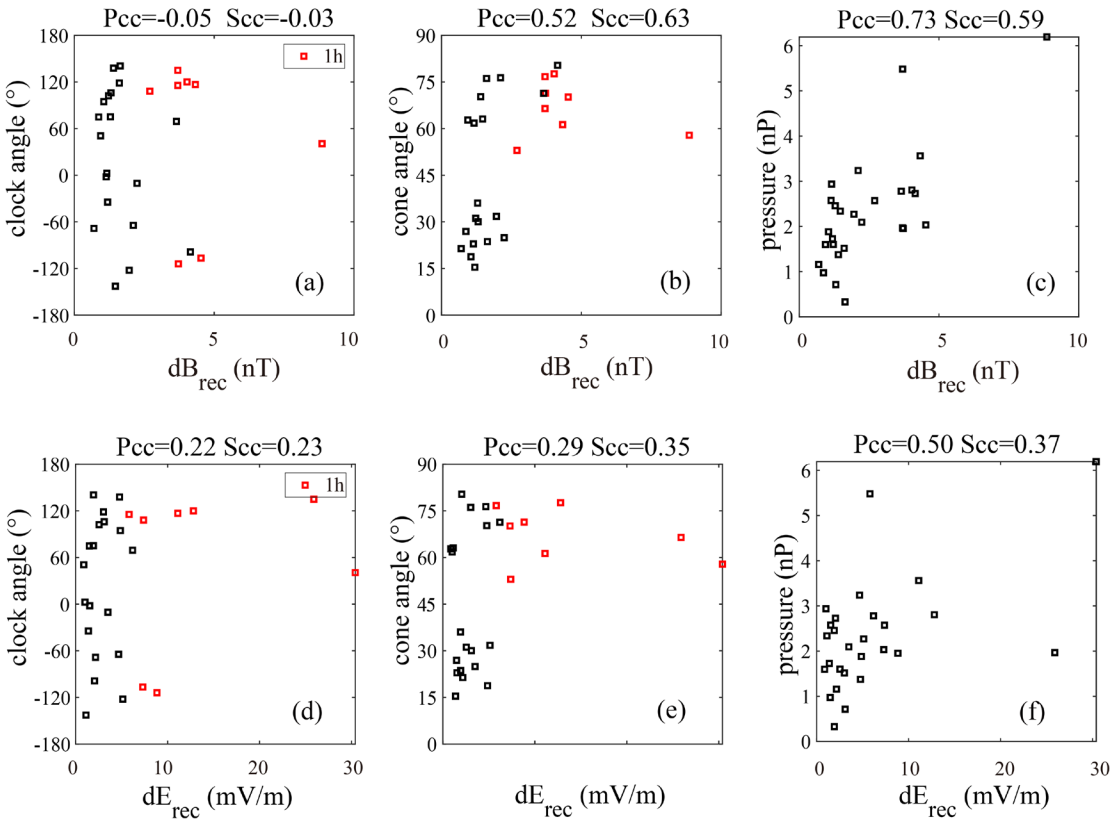

892

893 **Figure 6.** dB_{rec} and dE_{rec} for the turbulent reconnections versus solar wind conditions.
894 (a, d) IMF clock angle, (b, e) IMF cone angle, and (c, f) solar wind dynamic pressure.
895 The red and black squares in Figures a,b,d, and f indicate the LRs and PSRs,
896 respectively. Here, the clock angle is defined as $\tan^{-1}(B_y, B_z)$, cone angle is defined as
897 $\cos^{-1}(B_y/|\mathbf{B}|)$

898

899 **Figure 7**

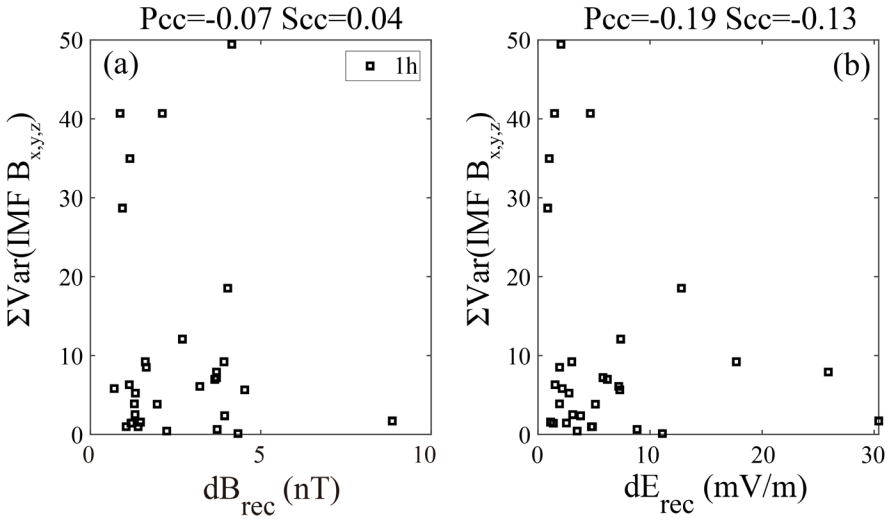

900

Figure 7. Scatter plot of dB_{rec} (a) and dE_{rec} (b) versus the aggregate of variances within the components of IMF $\sum_{i=x,y,z} Var(IMF\ B_i)$.

Figure 8

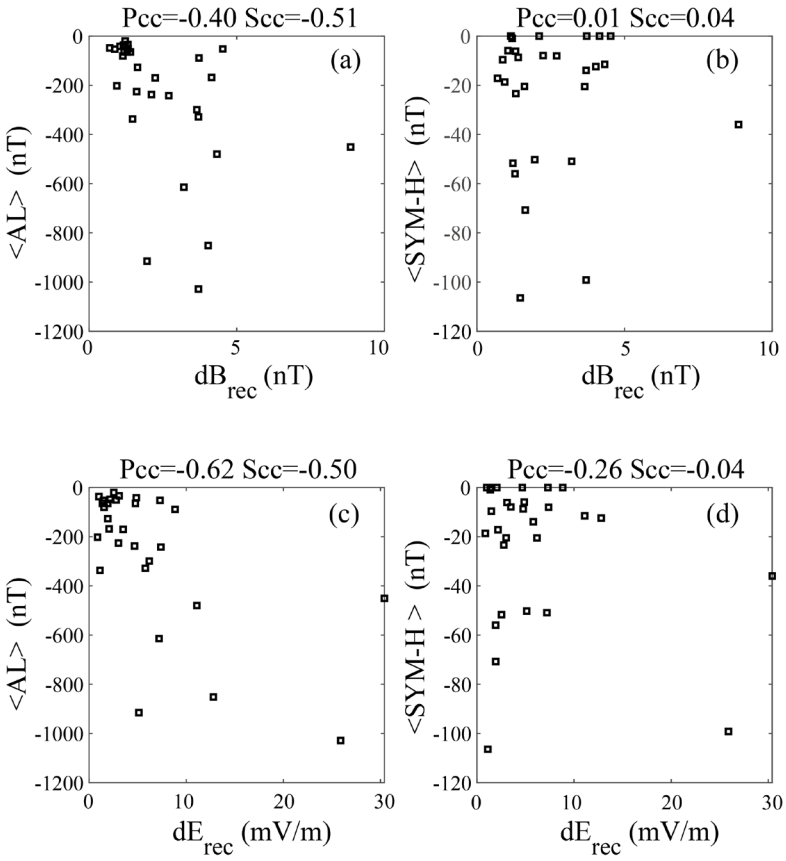

Figure 8. Scatter plot of dB_{rec} and dE_{rec} for the turbulent reconnections versus the averaged (a, c) AL index and (b, d) SYM-H index.

Figure 1.

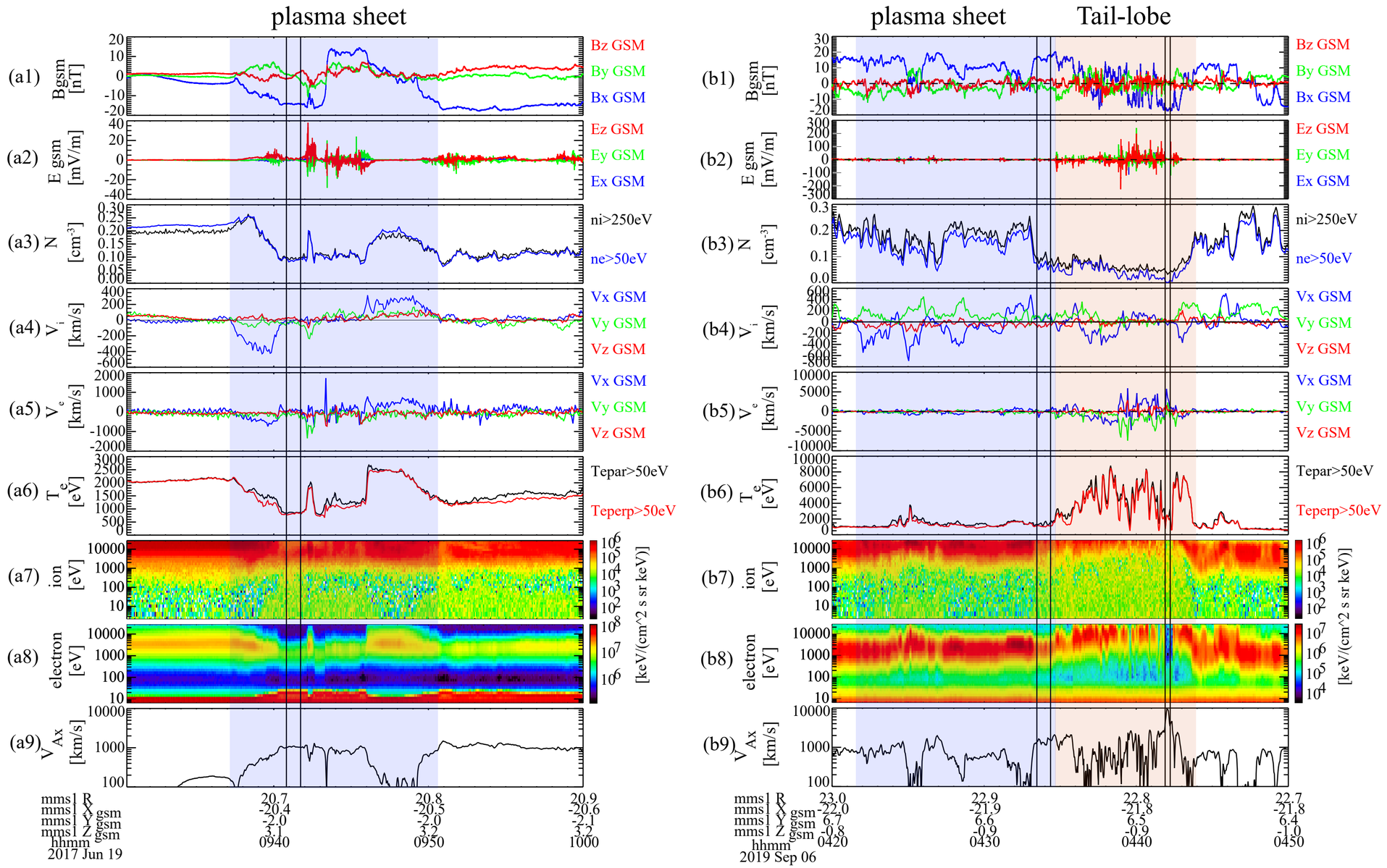
plasma sheet
plasma sheet
Tail-lobe
(a1)
Bgsm [nT]
Bz GSM
By GSM
Bx GSM
(a2)
E gsm [mV/m]
Ez GSM
Ey GSM
Ex GSM
(a3) N [cm-3]
ni>250eV
ne>50eV
(a4) Vi [km/s]
Vx GSM
Vy GSM
Vz GSM
(a5) Ve [km/s]
Vx GSM
Vy GSM
Vz GSM
(a6) Te [eV]
Tepar>50eV
Teperp>50eV
(a7) ion [eV]
[keV/(cm^2 s sr keV)]
(a8) electron [eV]
(a9) VAx [km/s]
mms1 R 20.7 20.8 20.9
mms1 X gsm -20.4 -20.5 -20.6
mms1 Y gsm -2.0 -2.0 -2.1
mms1 Z gsm 3.1 3.2 3.2
hhmm 0940 0950 1000
2017 Jun 19
(b1)
Bgsm [nT]
Bz GSM
By GSM
Bx GSM
(b2)
E gsm [mV/m]
Ez GSM
Ey GSM
Ex GSM
(b3) N [cm-3]
ni>250eV
ne>50eV
(b4) Vi [km/s]
Vx GSM
Vy GSM
Vz GSM
(b5) Ve [km/s]
Vx GSM
Vy GSM
Vz GSM
(b6) Te [eV]
Tepar>50eV
Teperp>50eV
(b7) ion [eV]
[keV/(cm^2 s sr keV)]
(b8) electron [eV]
(b9) VAx [km/s]
mms1 R 23.0 22.9 22.8 22.7
mms1 X gsm -22.0 -21.9 -21.8 -21.8
mms1 Y gsm 6.7 6.6 6.5 6.4
mms1 Z gsm -0.8 -0.9 -0.9 -1.0
hhmm 0420 0430 0440 0450
2019 Sep 06

Figure2.

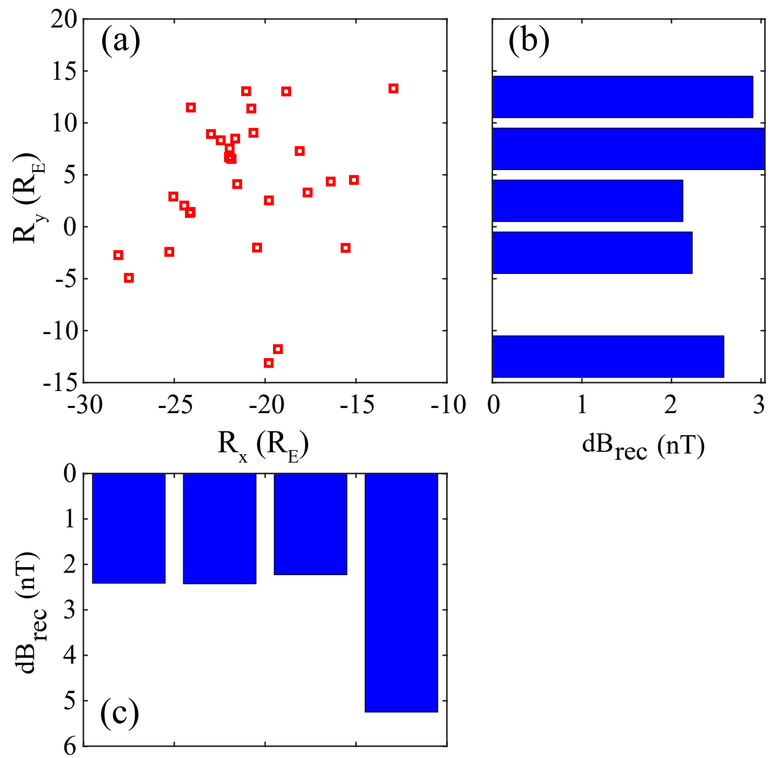
(a)
(b)
(c)
R_y (R_E)
R_x (R_E)
dB_{rec} (nT)
dB_{rec} (nT)
20
15
10
5
0
-5
-10
-15
-30
-25
-20
-15
-10
0
1
2
3
0
1
2
3
4
5
6

Figure3.

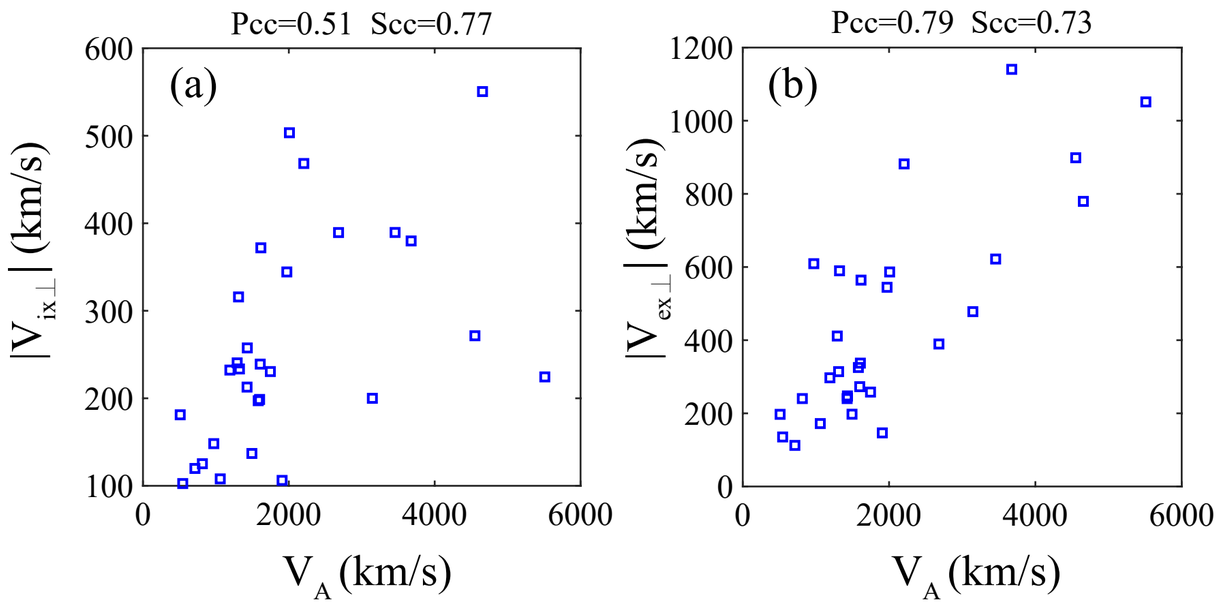
Pcc=0.51 Scc=0.77
(a)
600
500
400
300
200
100
0
2000
4000
6000
$|V_{ix\perp}|$ (km/s)
V_A (km/s)
Pcc=0.79 Scc=0.73
(b)
1200
1000
800
600
400
200
0
2000
4000
6000
$|V_{ex\perp}|$ (km/s)
V_A (km/s)

Figure4.

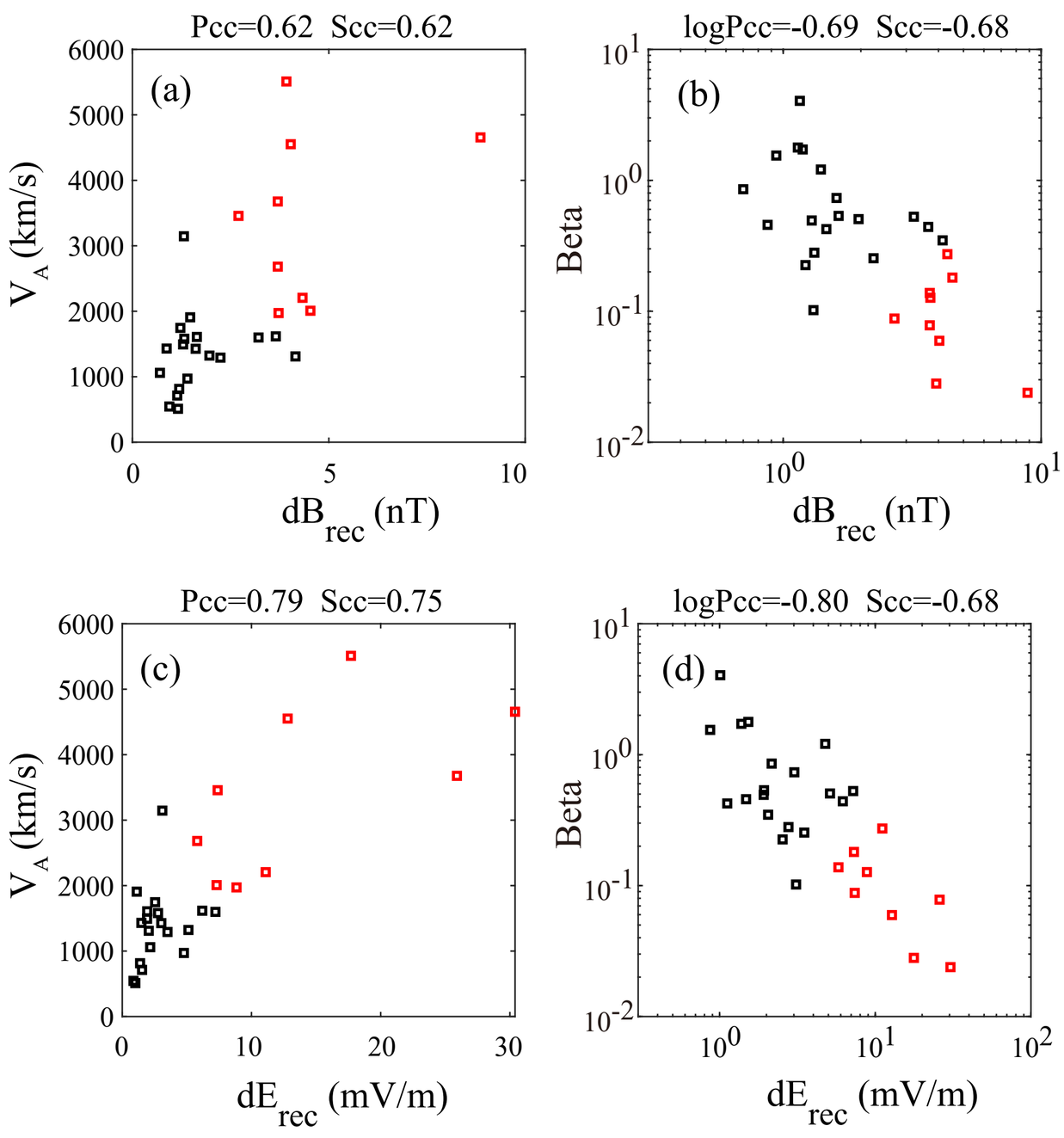
Pcc=0.62 Scc=0.62
(a)
V_A (km/s)
6000
5000
4000
3000
2000
1000
0
0
5
10
dB_{rec} (nT)
logPcc=-0.69 Scc=-0.68
(b)
Beta
10^1
10^0
10^{-1}
10^{-2}
10^0
10^1
dB_{rec} (nT)
Pcc=0.79 Scc=0.75
(c)
V_A (km/s)
6000
5000
4000
3000
2000
1000
0
0
10
20
30
dE_{rec} (mV/m)
logPcc=-0.80 Scc=-0.68
(d)
Beta
10^1
10^0
10^{-1}
10^{-2}
10^0
10^1
10^2
dE_{rec} (mV/m)

Figure5.

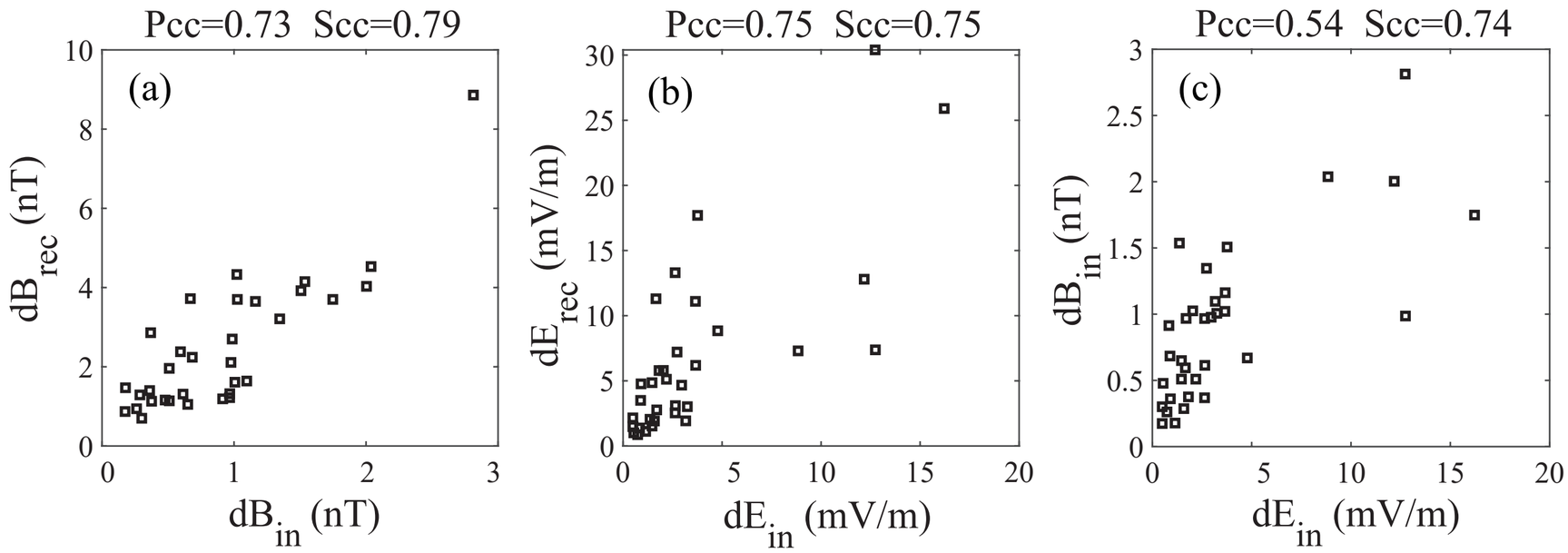
Pcc=0.73 Scc=0.79
(a)
dB_rec (nT)
dB_in (nT)
Pcc=0.75 Scc=0.75
(b)
dE_rec (mV/m)
dE_in (mV/m)
Pcc=0.54 Scc=0.74
(c)
dB_in (nT)
dE_in (mV/m)
Pcc=-0.10 Scc=-0.14
(d)
dB_rec (nT)
<acos(B_in ·<B_in>)> (°)
Pcc=0.41 Scc=0.47
(e)
dB_rec (nT)
dB_ps (nT)
Pcc=0.38 Scc=0.40
(f)
dE_rec (mV/m)
dE_ps (mV/m)

Figure6.

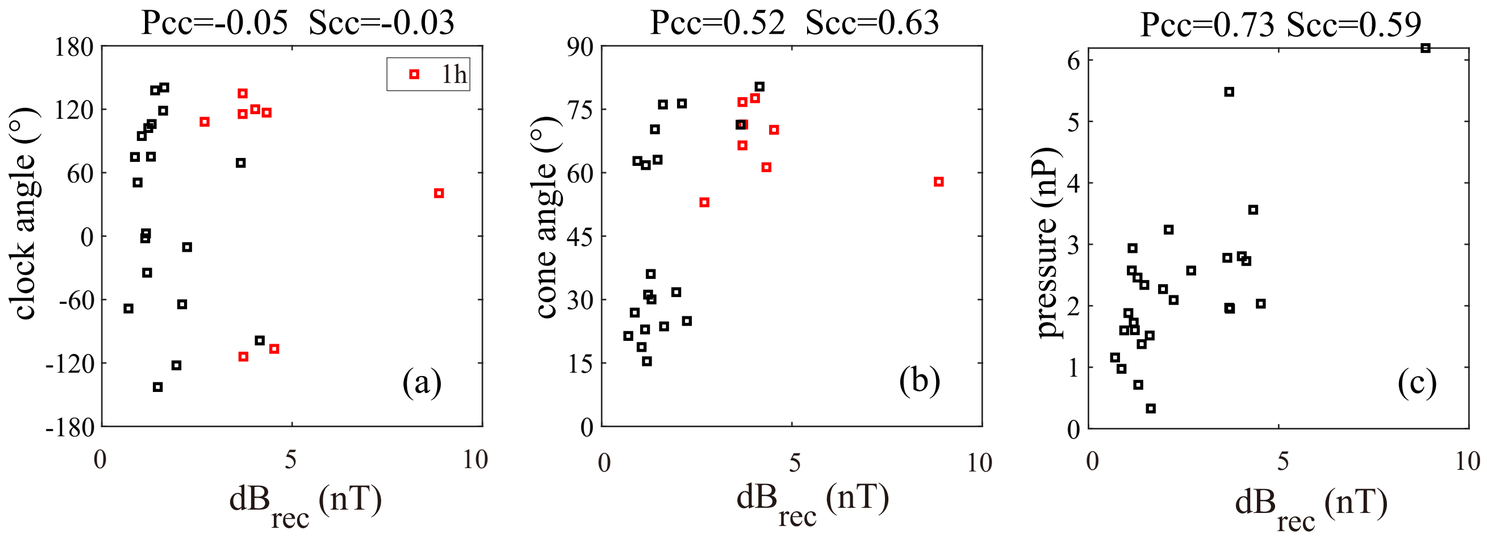
Pcc=-0.05 Scc=-0.03
Pcc=0.52 Scc=0.63
Pcc=0.73 Scc=0.59
1h
clock angle (°)
cone angle (°)
pressure (nP)
dB rec (nT)
(a)
(b)
(c)
Pcc=0.22 Scc=0.23
Pcc=0.29 Scc=0.35
Pcc=0.50 Scc=0.37
dE rec (mV/m)
(d)
(e)
(f)

Figure7.

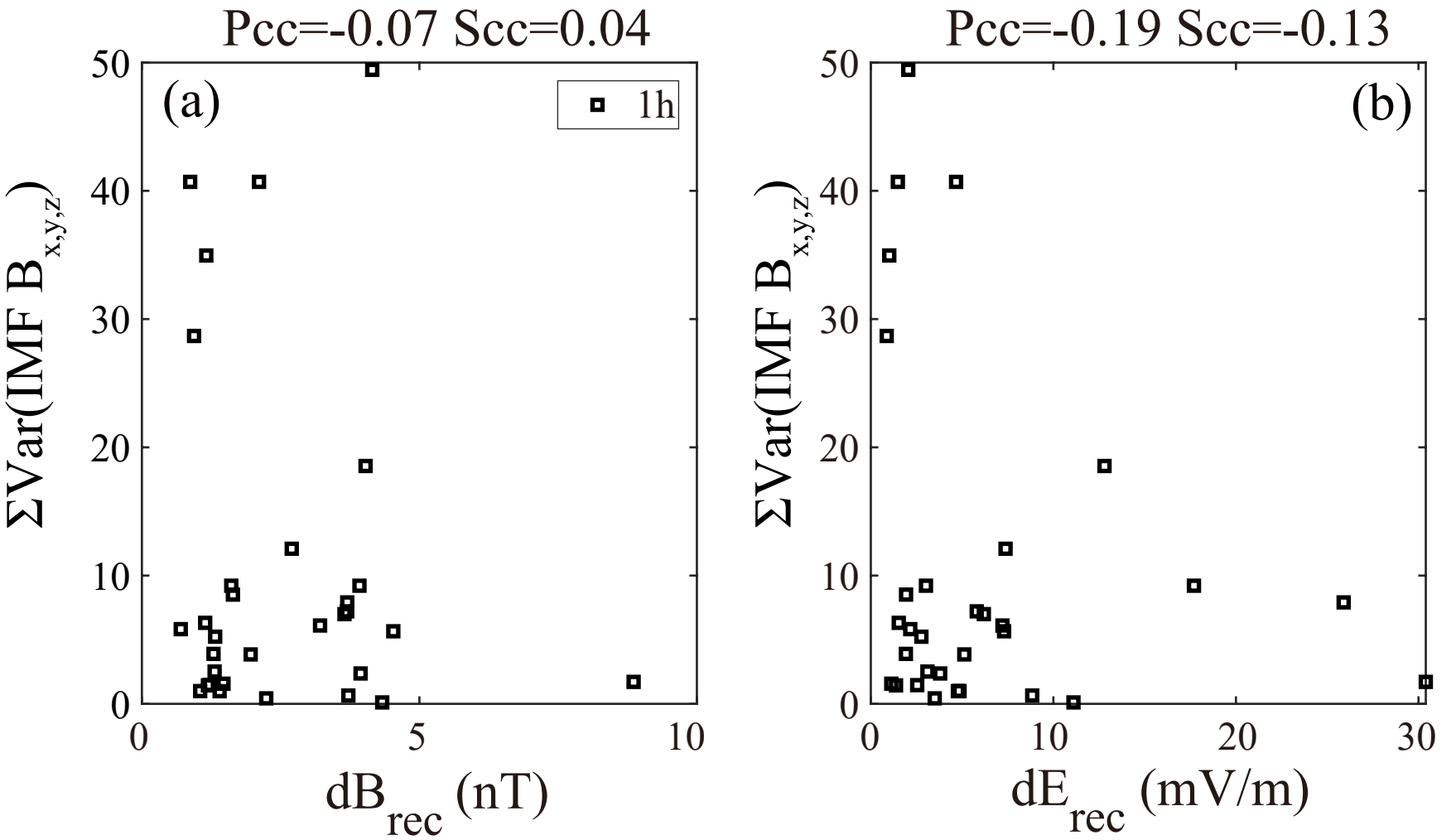
Pcc=-0.07 Scc=0.04
(a)
1h
ΣVar(IMF B x,y,z)
dB rec (nT)
0
5
10
20
30
40
50
Pcc=-0.19 Scc=-0.13
(b)
ΣVar(IMF B x,y,z)
dE rec (mV/m)
0
10
20
30
40
50

Figure8.

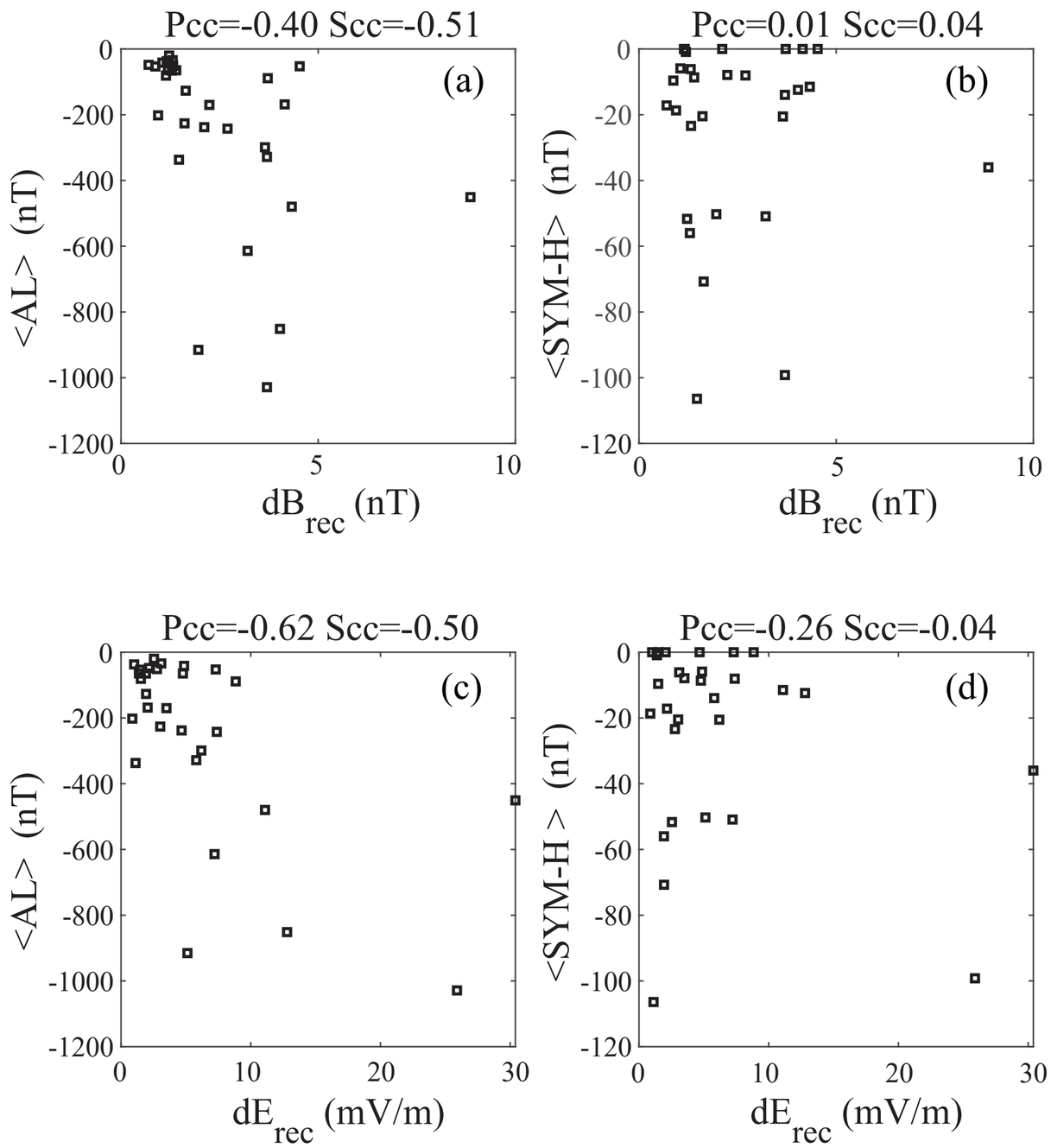
Pcc=-0.40 Scc=-0.51
(a)
<AL> (nT)
dB$_{rec}$ (nT)
Pcc=0.01 Scc=0.04
(b)
<SYM-H> (nT)
dB$_{rec}$ (nT)
Pcc=-0.62 Scc=-0.50
(c)
<AL> (nT)
dE$_{rec}$ (mV/m)
Pcc=-0.26 Scc=-0.04
(d)
<SYM-H > (nT)
dE$_{rec}$ (mV/m)